DEVELOPMENT OF SELF-ALIGNED INTERDIGITATED ELECTRODES WITHIN A MICROFLUIDIC CHANNEL FOR AN ELECTROCHEMILUMINESCENCE SENSOR

A Thesis

Presented to

the Faculty of the Department of Electrical and Computer Engineering

University of Houston

In Partial Fulfillment

of the Requirements for the Degree

Master of Science

in Electrical Engineering

by

Gauri Samel

December 2012

DEVELOPMENT OF SELF-ALIGNED INTERDIGITATED ELECTRODES WITHIN A MICROFLUIDIC CHANNEL FOR AN ELECTROCHEMILUMINESCENCE SENSOR

Gauri Anil Samel

Approved:

Chair of the Committee
Paul Ruchhoeft, Associate Professor
Electrical and Computer Engineering

Committee Members:

Dmitri Litvinov, Professor
Electrical and Computer Engineering

Richard Willson, Professor
Chemical and Biomolecular Engineering

Suresh K. Khator, Associate Dean
Cullen College of Engineering

Badrinath Roysam, Professor and Chair
Electrical and Computer Engineering

Acknowledgements

I would like to thank my advisor Dr. Paul Ruchhoeft for all his guidance and advice throughout the project and acknowledge Dr. Dmitri Litvinov and Dr. Richard Willson for being the committee members on my project. I would also like to thank Dr. Shivakumar Bhaskaran and Dr. Kelley Bradley for training me on the clean room equipment. Moreover, I would like to express my gratitude towards my labmates, Tim Sherlock, David Shakarisaz, and Carmen Pascente, as well as several other graduate students, Anupam Aich, Nikhil Dole, Ivan Nekrashevich, and Ashish Tripathi for all their suggestions and help with the project. Finally, I would like to thank my parents, Anil and Nutan Samel, and my older sister, Dipti, for supporting me financially as well as emotionally.

DEVELOPMENT OF SELF-ALIGNED INTERDIGITATED ELECTRODES WITHIN A MICROFLUIDIC CHANNEL FOR AN ELECTROCHEMILUMINESCENCE SENSOR

An Abstract

of a

Thesis

Presented to

the Faculty of the Department of Electrical and Computer Engineering

University of Houston

In Partial Fulfillment

of the Requirements for the Degree

Master of Science

in Electrical Engineering

by

Gauri Samel

December 2012

Abstract

The aim of this work was to develop a fabrication sequence for forming microchannels with integrated, interdigitated electrodes using only one lithographic step as a platform for developing electrochemiluminescence biosensors. The microfluidic channels and electrode structures are formed by contact lithography using a negative tone photoresist (SU-8), and the pattern contains both the channel structure and an array of walls that are 4 mm long, 20 microns wide, 50 microns tall and are spaced 50 microns apart from each other. The electrodes are formed by coating metal on the walls of the polymer by electron beam evaporation through a mask by tilting the substrate on both sides at an angle, thereby allowing for a large selection of electrode materials without the need for multiple lithographic steps or the need to directly pattern the metal. The approach takes advantage of the geometry of the pattern to coat only the sidewalls of the polymer without electrically connecting them through the base of the channel.

Table of Contents

List of Figures

Chapter 1

Introduction

Microfluidic devices contain microchannels that involve fluids with a volume in the range of nL and pL [1]. The dimensions for these channels are less than 1 mm. In such small channels, it is easier to manipulate and control the behavior of fluids due to laminar flow of the fluids and micro-scale dimensions of the channel. Such systems are cost-effective since, they require significantly smaller volumes of fluids and reagents for reactions [2, 3]. With these devices, the need for expensive equipment can be reduced, as one small microchip is used to perform several functions, like detection of a particular component in the fluid or analysis of the fluid [4]. Micro-channel devices offer several advantages when compared to fluids flown through macro-channels, including a smaller fluid volume, potentially lower fabrication costs, better control over fluid flow, and increased sensitivity. The major application area for microfluidic devices is in bio-industry for detection and analysis purpose. Fluids that flow through these devices include blood, buffers, protein solutions, etc. [2].

There are several techniques for making microfluidic channels, such as reactive/deep reactive ion etching, where the substrate is etched up to a certain depth to define the channel height, soft lithography wherein channels are formed in PDMS, electro-chemical deposition, laser ablation, etc. [4]. However, the simplest technique to fabricate a microchannel is by using two cover slips and a double sided adhesive tape, where one of the cover slips will have two drilled holes. These holes act as ports for pumping the liquid in and out of the channel. A double sided adhesive tape is placed on the other cover slip. The cover slip with ports is placed on the taped cover slip so that they remain firmly attached. The liquid can now flow from the inlet port into the gap between the slips. The gap between the slips is formed due to the thickness of the double

sided adhesive tape. Figure 1, shows the channel obtained with cover slips and double-sided adhesive tape. Electrodes can be integrated on this channel by evaporating metal on the cover slip.

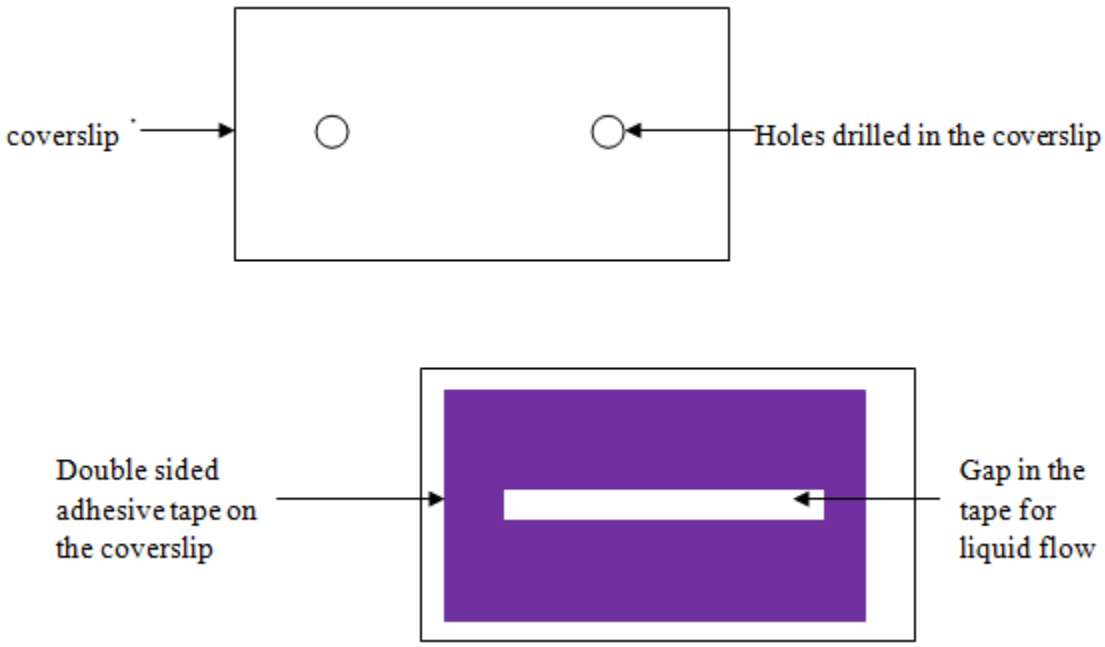

Figure 1. A simple technique of forming microfluidic channel using glass cover slip and double-sided adhesive tape.

In this project, the double-sided adhesive tape is omitted and, the microfluidic channel is formed by spin coating a photoresist on a substrate. The resist is baked, patterned and developed to define the channel boundary and form an inter-digitated array of polymer walls. The array of walls is coated with metal by double-angled evaporation technique. This evaporation technique is also used to form positive and negative electrode.

After performing fabrication steps to form the channel, resistance of two solutions with known resistivity are flown through the channel. The two liquids are de-ionized water and phosphate buffered saline. The resistance of these two liquids is measured by an ohmmeter whose

probes are connected across the metal electrodes that are formed by angular evaporation. Air resistance is also measured when no liquid is dispersed in the channel. The resistance values of air, de-ionized water and buffer solution are compared to test that the electrodes formed do not short internally. The 3-D view of the microfluidic channel formed in this project is shown in Figure 2. It consists of an inlet and outlet port to pump the fluid in and out of the channel and a sensor region wherein all the detection takes place.

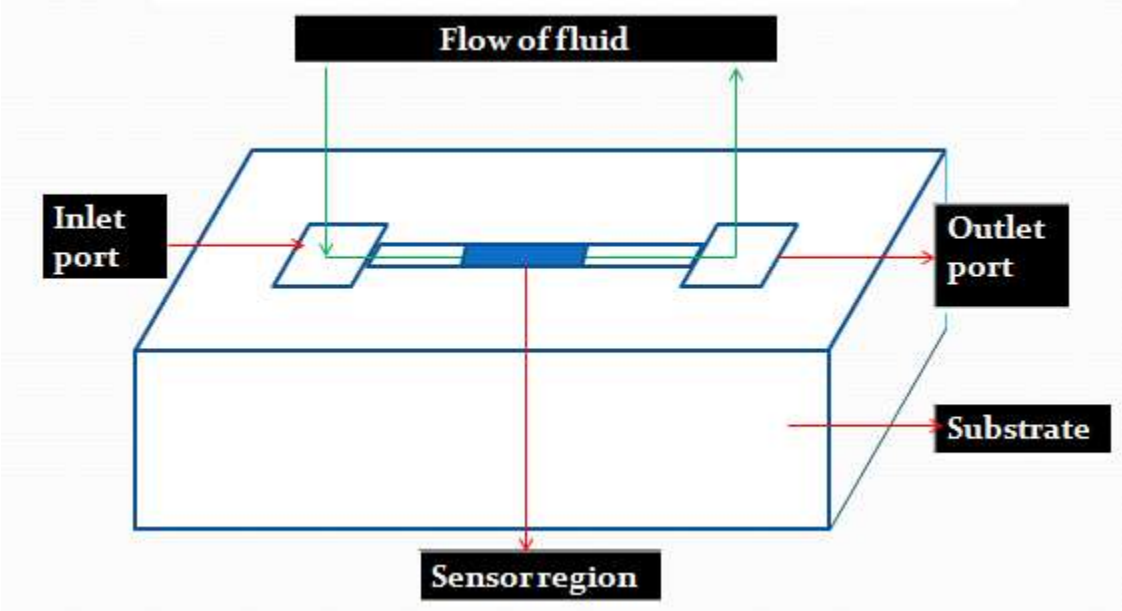

Figure 2. Microfluidic channel with inlet and outlet port on substrate.

1.1 The Electrochemiluminescence Effect

In this project, the fabricated microfluidic channel can potentially be used as an ECL sensor. The electrochemiluminescent effect occurs within the channel as seen in Figure 3.

(a) The channel consists of an inlet and outlet port along with a sensor region. The sensor region is comprised of several inter-digitated structures of SU-8 walls that are coated with metal to act as electrodes. Two such electrodes are shown in the figure for understanding the ECL effect within the channel.

(b) The channel walls are decorated with antibodies that specifically capture the target antigen. For example, if a bacterium is to be detected in the sample, the channel walls will contain bacterial antibodies. Antibodies are ‘Y’ shaped and consists of paratope at its two tips whereas an antigen consists of an epitope, to which the paratope binds. Each antibody binds to a specific antigen.

(c) A fluid is flown through the channel which consists of the antibody specific antigen as well as several other components. When the particular antigen comes in contact with the antibody, the antibody captures it, i.e., a bond is formed between the antibody and the attached antigen. A wash step is performed to remove the fluid along with other components from the channel so that the channel would now only contain the links of antibody-antigen. This is also done to ensure that there would be no interference in the chemical reaction for ECL due to any other molecules present in the channel.

(d) A solution, containing the same type of antibody which is deposited on the wall, attached to a label, is injected in the channel. In this case, the label is an electrochemiluminescent molecule. On coming in contact with the antigen, the labeled antibody binds to the antigen which was previously captured by the primary antibody. Thus, a link of primary antibody-pathogen-labeled antibody-electrochemiluminescent molecule is formed on the walls of the channel. A wash step is performed to remove any unattached labeled antibody from the channel.

(e) A suitable voltage is applied across the electrode, which creates an electric field between the adjacent channel walls. This is because; the walls are alternately connected to the positive or the negative electrode.

(f) In the presence of an electric field, the ECL molecule undergoes a chemical reaction, which causes the electrons to move to an excited state. The excited state then returns to the ground state and releases a photon. The release of photons from the ECL molecules causes a glow if the pathogen is captured since; the pathogen is linked to the antibody which in turn is attached to the ECL molecule. The glow also indicates the presence of pathogen if it is properly bound to

the antigen. The color of the glow depends on the ECL molecule used and the wavelength of light emitted. The process of generating ECL, the molecules used for ECL process, and the chemical reactions involved in it are explained in detail in Chapter 2.

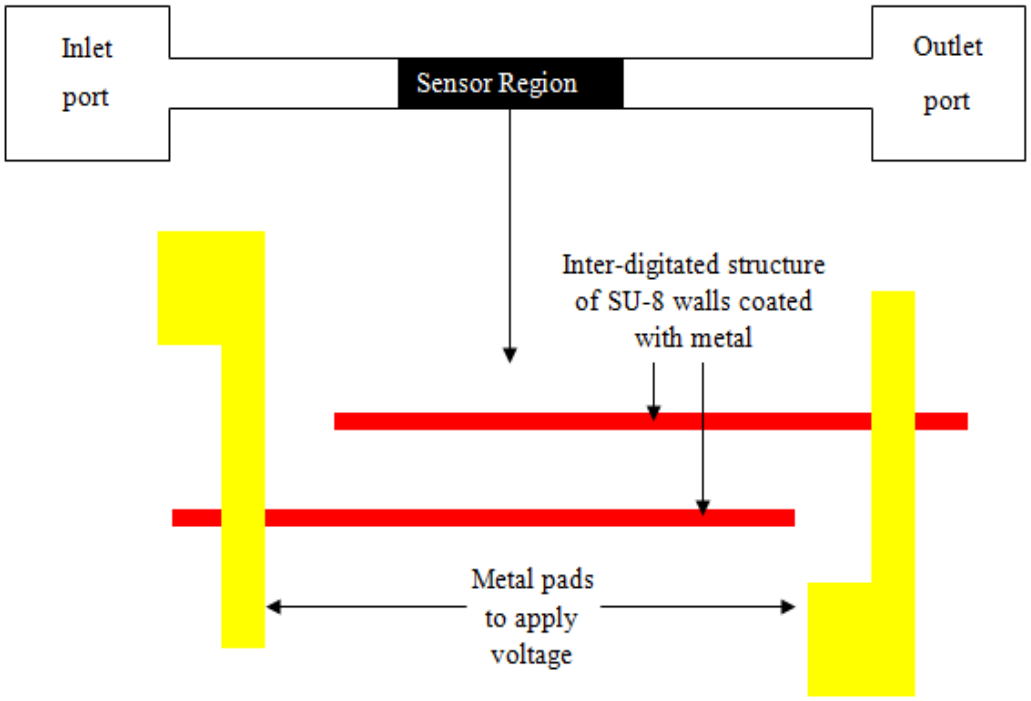

(a)

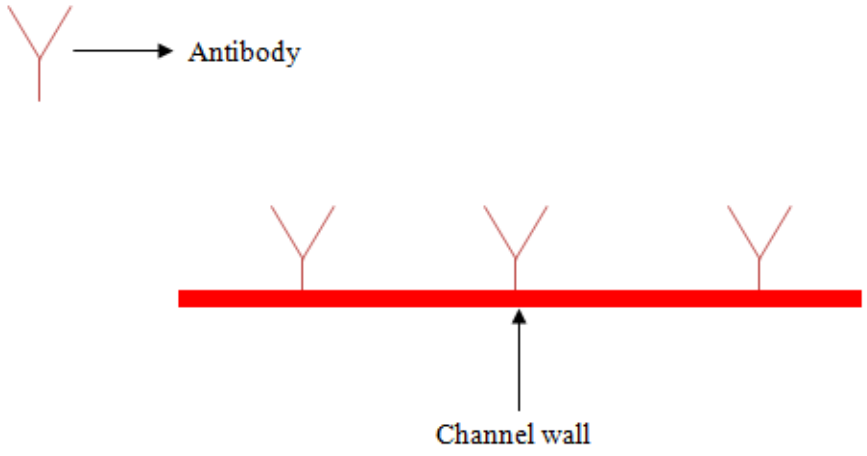

(b)

Figure 3. (a-f) ECL effect in the microfluidic channel (a) Microfluidic channel with inter-digitated metal electrodes. (b) Antibodies immobilized on the channel walls.

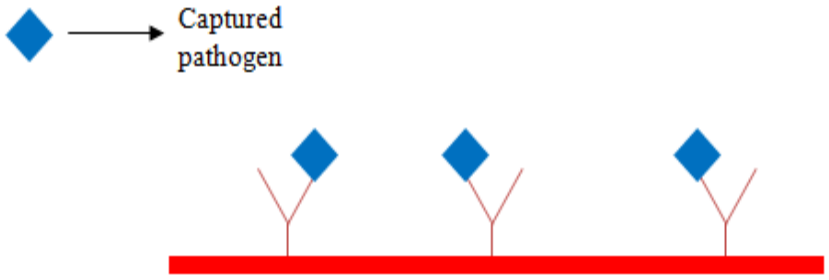

(c)

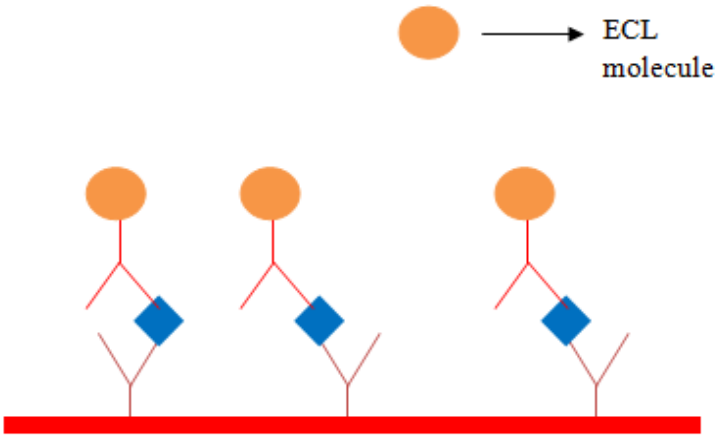

(d)

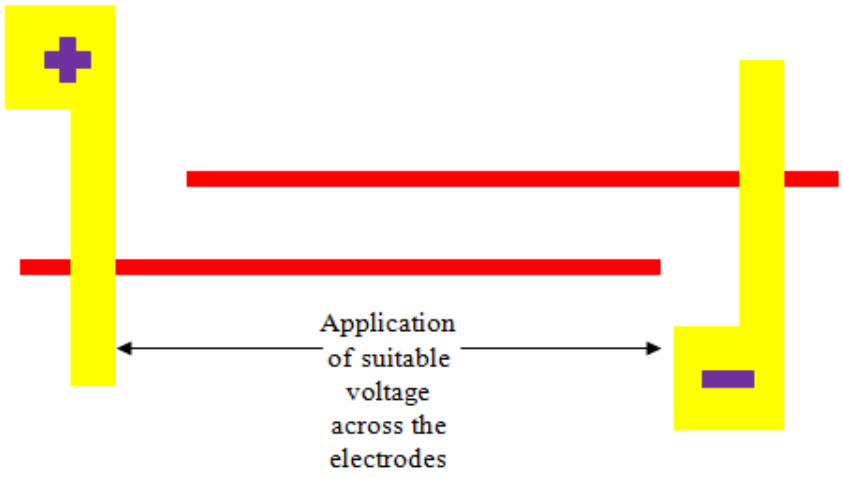

(e)

Figure 3. (a-f) ECL effect in the microfluidic channel. (c) Pathogen is captured by the antibody. (d) Antibody with electrochemiluminescent label gets linked to the pathogen. (e) Voltage is applied across the electrodes.

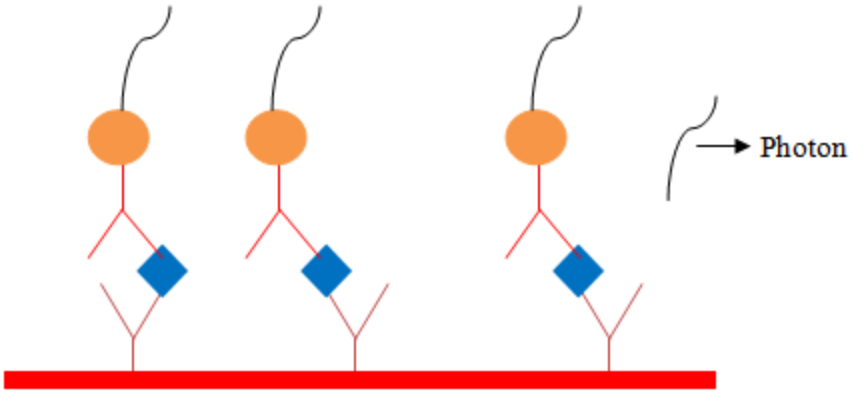

(f)

Figure 3. (a-f) ECL effect in the microfluidic channel. (f) Application of voltage causes the ECL molecule to undergo a reaction that releases a photon.

1.2 Overview of the Thesis

In this project, a microfluidic channel is fabricated using lithography steps and angular evaporation. Chapter 2 explains the photoresist used for fabrication, which is SU-8, including its application and advantages. It provides an overview of other labeling techniques. It also discusses methods of generating ECL as well as the chemical reactions involved in the process. It looks into the various techniques of fabricating microfluidic channels with electrodes. The magnetic bead method for detection of pathogen in the channel via ECL is also described.

Chapter 3 describes experimental set-up that was used to fabricate the microchannel. It describes the parameters, procedures, steps and techniques that were used to form the channels. The fabrication steps used were spin coating, baking, contact lithography, and developing the substrate. It explains a technique of coating the channel walls with metal, called the double-angled evaporation technique. It also explains the working of several equipment such as spin coater, mask aligner and electron beam evaporator that were used in the project. The method for measuring resistance is covered in this chapter.

Chapter 4 details the results that were obtained after performing the experiments mentioned in Chapter 3. It explains the issues experienced while fabricating the microchannels, which includes under-exposure, stress in the resist, and shorting of the electrodes. The change in design of the mask and its dimensions to overcome the issues is covered in this chapter. It discusses the optical microscope images taken after performing double angled evaporation that causes the SU-8 fin to cast a shadow up to a distance which is decided by the angle set in the equipment. It also discusses the calculated and observed resistance values of two standard liquids to verify that the electrodes thus formed do not short internally.

The thesis concludes with Chapter 5, which summarizes the work. Future-work for scaling the device, sealing the channel, as well as modifications that can be done in the present channel to test it for an ECL sensor are described.

Chapter 2

Literature Review

2.1 SU-8 Photoresist

The polymer selected for fabricating micro-channels is SU-8 photoresist. It is a negative–tone, chemically amplified epoxy resist and is very sensitive for wavelengths of light from 350-400 nm. It was developed and patented by IBM [5]. It is comprised of three basic components; the epoxy, a solvent, and acid generator/photo-active compound (triarylsulfonium salt). SU-8 contains 8 epoxy or polyepoxide groups per molecule. The solvent used is GBL (gamma-butyrolacton), which dissolves the resin. The amount of added solvent controls the viscosity of the resist as well as the different thicknesses that can be obtained with the resist. The acid generator/photoinitiator is added to the polymer by the vendor [6]. When the resist is exposed to UV light, acid is released. The acid produced in the exposure step, initiates the cross-linking process during post-exposure bake.

SU-8 yields thermally, chemically, and mechanically stable structures after cross-linking. It is known to give very high aspect ratio structures. A single spin coat step can provide structures up to 200 microns whereas multiple spin coating step can provide structures up to 3 mm. It is extremely bio-compatible, has a low-cost, and provides no environmental or health hazards. Vertical sidewalls can be obtained with this resist. It can also be used with e-beam and x-ray lithography. It is used as a mask for reactive ion etching of silicon [7]. Another advantage of SU-8 is that it does not require high temperature treatment in the process of micro and nanostructure formation or any special storage conditions [5].

2.2 Electrochemiluminescence Effect in Microfluidics

Bio-sensors rely on biochemical sensing mechanism between the molecules of interest. The most common forms of sensing in the bio-sensors are based on the interaction between an antibody and its corresponding antigen. The antigen binds to the antibody in a lock and key fashion [8]. As mentioned in Chapter 1, for ECL to occur, a link needs to be formed between a primary antibody, antigen, and a labeled antibody, where the label is an electrochemiluminescent molecule.

There are several labeling techniques used such as fluorescence labeling, radio-active labeling, electrochemiluminescence labeling, etc. In radio-active labeling, the labeled molecule is radioactive, that keeps on emitting radiation, which can then be detected by a radiation detector such as Geiger Muller or scintillation counter. However, the radiation emitted is harmful to the human body and cost of manufacturing is also very high [8]. In the fluorescence technique, a label molecule, which is known as a fluorophore, is attached to the protein. The molecule glows or fluoresces upon being excited by light. The excitation and emission wavelength depends on the fluorophore used. However, there are some disadvantages with the fluorescent technique. Firstly, there can be interference due to ambient light, which can be resolved by placing the fluorescent equipment in a dark box. However, that complicates the device structure and increases the overall cost of the system. Secondly, if a low-cost filter is used, it may allow too much light at the excitation wavelength to reach the detector, thus degrading the signal-to-noise ratio [9]. Due to the mentioned disadvantages with the two methods, research is focused towards developing other low-cost, safe and highly efficient techniques.

ECL or Electro-generated Chemiluminescence is so named since the luminescence occurs due to a chemical reaction which is generated by an electric field. With electrochemiluminescence, all the disadvantages mentioned with fluorescence and radio-active labeling techniques are eliminated, since it does not require a light source for excitation of the

ECL molecule nor does it emit any harmful radiation in the process. The ECL label is stable [10] and it keeps on emitting a photon as long as voltage is applied. It is a fast process [11] and is very cost-effective as there is no consumption of the label during the process. The most common molecule to perform ECL is ruthenium bypyridine, $Ru(bpy)_3^{2+}$. It emits photons at 620 nm [12], giving a yellow-orange color when it glows. A molecule rubrene [13] and a reagent luminol [14], are also known to generate ECL.

The following mechanism for generating ECL is referenced from [15]. ECL is generated by annihilation or by introducing a co-reactant in the solution. In annihilation ECL, the ECL molecule undergoes a chemical reaction to produce its oxidized and reduced species. These two produced species react with each other to form an excited state of the ECL molecule. The excited ECL state returns to ground state with the release of a photon. The oxidized and reduced ECL species can be produced on the same electrode or different electrodes. However, if they are produced at different electrodes, then the electrodes need to be very close to each other so that the produced species can diffuse and react to form the excited state. For producing the species at same electrode, alternate pulsing of voltage is required. The chemical reactions that occur for generating ECL via annihilation are as follows:

$$R - e^- \rightarrow R^+, \tag{1-a}$$

$$R + e^- \rightarrow R^-, \tag{1-b}$$

$$R^+ + R^- \rightarrow R^0 + R, \tag{1-c}$$

$$R^0 \rightarrow R + h\upsilon, \tag{1-d}$$

where, R is the ECL molecule, R^+ is the oxidized species, R^- is the reduced species, e^- is electron, R^0 is excited state, and $h\upsilon$ is the emitted photon (h is Planck's constant and υ is the frequency).

In co-reactant ECL, a co-reactant compound is introduced in the ECL solution which either oxidizes or reduces to produce an intermediate state. The intermediate state reacts with the oxidized or reduced ECL luminophore, respectively, to produce an excited state. The excited state returns to ground state releasing a photon in the process. Hence, with a co-reactant, ECL occurs via oxidative-reductive or reductive-oxidative mechanism of the co-reactant and ECL molecule. The most common co-reactant used for oxidative-reductive reaction is tri-propylamine (TPrA) whereas for reductive-oxidative reaction it is peroxy-disulfate ($S_2O_8^{2-}$). The chemical reaction for TPrA considering Ruthenium bipyridine as the ECL species is discussed below:

$$Ru(bpy)_3^{2+} - e^- \rightarrow Ru(bpy)_3^{3+}, \quad (2\text{-a})$$

$$TPrA - e^- \rightarrow TPrA^{0+} \rightarrow TPrA^0 + H^+, \quad (2\text{-b})$$

$$Ru(bpy)_3^{3+} + TPrA^0 \rightarrow Ru(bpy)_3^{2+*} + \text{product}, \quad (2\text{-c})$$

$$Ru(bpy)_3^{2+*} \rightarrow Ru(bpy)_3^{2+} + h\upsilon, \quad (2\text{-d})$$

where, $Ru(bpy)_3^{3+}$ is the oxidized state of Ru(bpy), $TPrA^{0+}$ is the oxidized state of TPrA, and $Ru(bpy)_3^{2+*}$ is the excited state.

Reductive-oxidative ECL mechanism with peroxy-disulfate as a coreactant occurs as follows:

$$Ru(bpy)_3^{2+} + e^- \rightarrow Ru(bpy)_3^{+}, \quad (3\text{-a})$$

$$S_2O_8^{2-} + e^- \rightarrow SO_4^{0-} + SO_4^{2-}, \quad (3\text{-b})$$

$$Ru(bpy)_3^{+} + SO_4^{0-} \rightarrow Ru(bpy)_3^{2+*} + SO_4^{2-}, \quad (3\text{-c})$$

$$Ru(bpy)_3^{2+*} \rightarrow Ru(bpy)_3^{2+} + h\upsilon, \quad (3\text{-d})$$

where $Ru(bpy)_3^{+}$ is the reduced state of $Ru(bpy)_3^{2+}$.

There are several ways in which ECL can be detected and one of the ways is by using magnetic bead method [9, 16, 17]. Magnetic beads coated with streptavidin [18] are discussed here as an example and is shown in Figure 4. Two antibodies of the same type, one labeled with ruthenium and the other labeled with biotin, which is a type of vitamin, are used. These two antibodies then bind to the same antigen. Para-magnetic beads functionalized with streptavidin, which is a type of protein, are introduced in the channel. Streptavidin has a tendency to form a strong bond with biotin. The entire solution which now contains several links of ECL molecule labeled with ruthenium-antigen-antibody with biotin streptavidin bond is now introduced in the ECL cell. The cell is equipped with electrodes and a magnet beneath it. The beads are attracted to the magnet due to magnetic field. The unlinked antibodies are removed from the channel by a wash step. A co-reactant solution is added to the channel. On application of a suitable voltage, the co-reactant and ruthenium undergo a chemical reaction to form products. The products react with each other to form an excited state, which returns to the ground state and releases a photon.

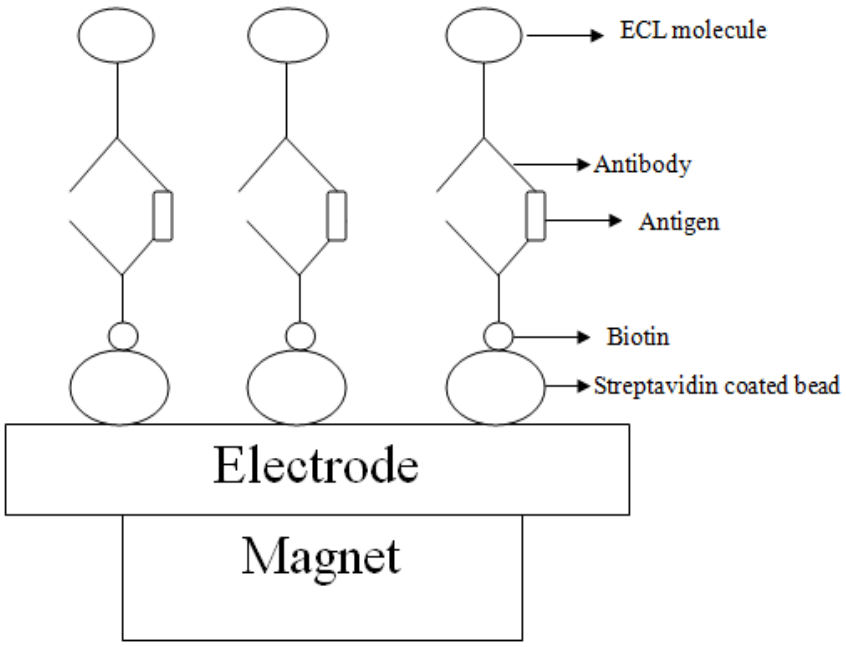

Figure 4. Magnetic Bead detection method for ECL via streptavidin coated magnetic bead-biotin-antigen-antibody-ECL molecule link.

2.3 Fabrication Methods of Microfluidic Channel

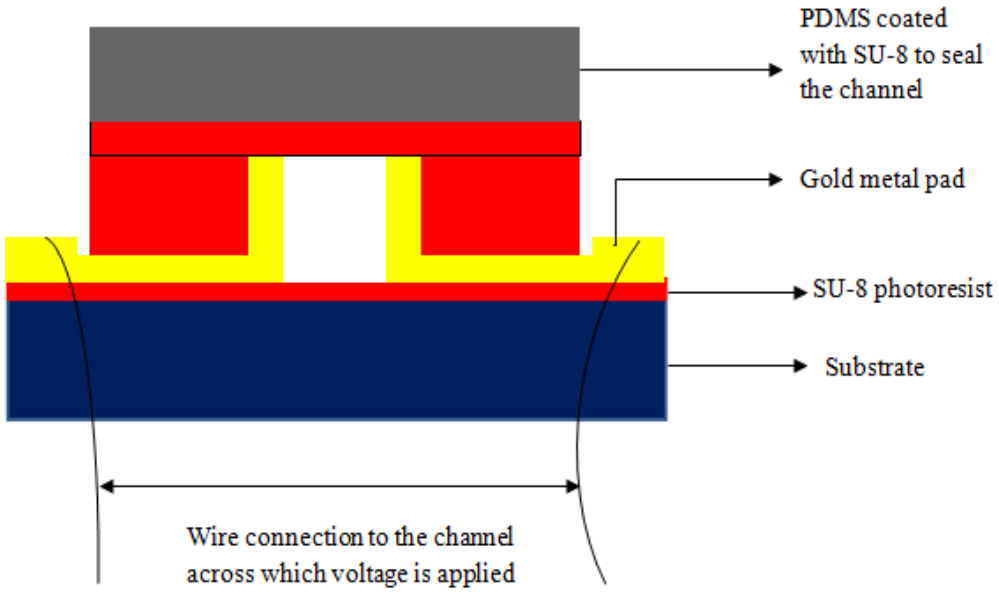

Figure 5. A sealed microfluidic channel on a silicon substrate with gold metal walls.

As mentioned in Chapter 1, there are several techniques of forming microchannels. Three methods of forming microchannels are discussed here. In the first technique, the channel is fabricated by optical lithography and electroplating, which forms tall vertical metal electrodes. In the second technique, the fabrication method used for forming the channels is by soft lithography and etching whereas the third technique explains fabrication of channels by electro-chemical methods using printed circuit board technology. For the first technique [19], a silicon substrate is used which is coated with 2 microns thick SU-8 photoresist. Gold is deposited on the substrate via electron beam evaporation. AZ photoresist is then spin coated on the substrate. Photolithography is performed to transfer the pattern of the mask on the resist. After developing the resist, few regions of the gold coated substrate are covered with resist whereas gold remains exposed on other regions of the substrate so as to form gold electrodes by electroplating. The parameters for electroplating process are set to obtain 30 micron tall metal structures. The AZ resist is stripped after electroplating gold and another layer of SU-8, which is 30 microns thick, is

patterned on the substrate, thus forming the microfluidic channel. To seal the channel, a glass slide is coated with Polydimethylsiloxane (PDMS) and SU-8. The PDMS and SU-8 is peeled from the glass slide and placed on the channel to seal the device. The channel obtained after the processing steps is shown in Figure 5.

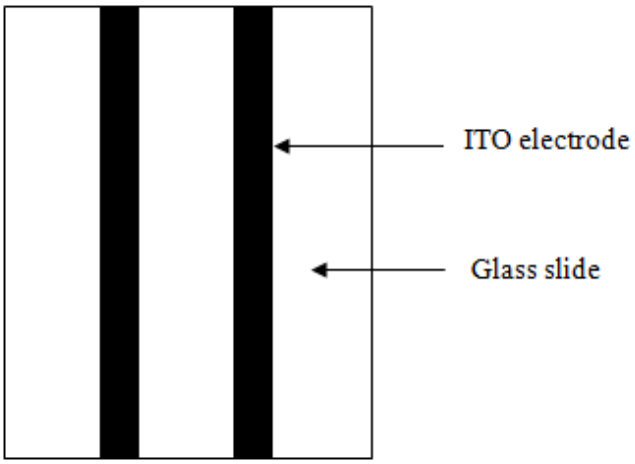

(a)

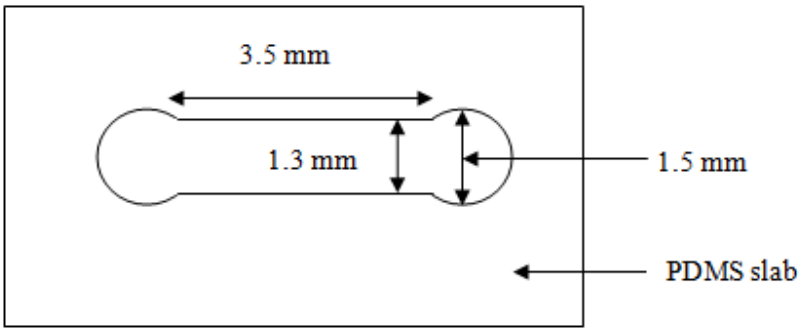

(b)

Figure 6. Microfluidic channel formed using soft lithography and etching. (a) Indium tin oxide electrodes on a glass slide. (b) Microfluidic channel formed in PDMS.

The second technique for forming microchannel, is described in reference [20]. To fabricate this microchannel, a glass slide was first patterned with photolithography and later with etching to obtain the desired pattern of the device as shown in Figure 6 (a). PDMS was poured on the patterned glass slide and was allowed to cool. On cooling, the PDMS was stripped and the

mold thus formed, was attached to an ITO coated glass slide. Carbon ink was filled in the PDMS mold that was attached to the ITO slide and the ink was allowed to dry. The PDMS mold was peeled from the ITO slide when the ink dried. A wet etching step was performed on the ITO coated glass with dried carbon ink. After etching, the ink was removed and the desired pattern of electrodes obtained on the ITO coated glass was rinsed and dried for further usage. The channel formed was sealed by another PDMS slab. The length, width and height of the slab were 3.5 mm, 1.3 mm and 30 microns respectively. It also contained inlet and outlet ports that were formed by drilling two holes of 1.5 mm in diameter as seen in Figure 6 (b). The PDMS slab was also formed by the same procedure as mentioned above.

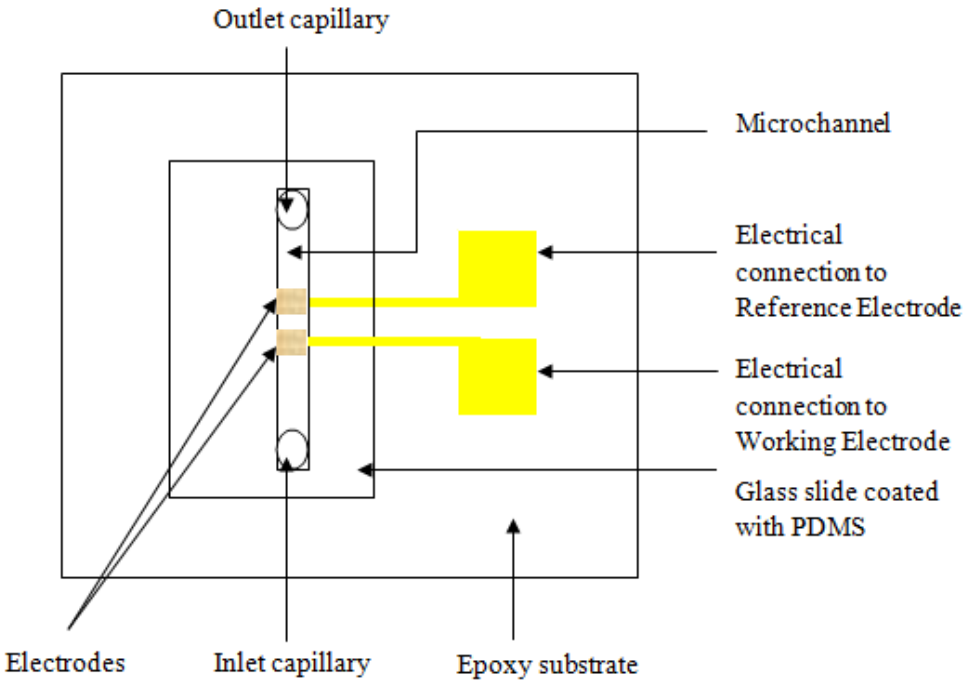

Figure 7. Microchannel formed using PCB technology. The channel consists of working and reference electrode and inlet and outlet capillary. The channel is sealed by a glass slide coated with PDMS.

In the third approach described here, an ECL microfluidic device has been fabricated using PCB (Printed Circuit Board) technology where an epoxy substrate with a solder mask was

used and the microfluidic channel was etched into the mask [21]. Electrodes were obtained by electroplating 80 nm gold on 35 microns of copper. Copper was used in the PCB to connect the circuit internally. The electrodes formed were 300 microns in length and width. Out of the two electrodes that were formed, one was selected to be the reference electrode whereas the other would hence, be a working electrode. The reference electrode was obtained by depositing a thin film of silver by electrochemical deposition on the gold plated copper. The channel was sealed with a glass slide that was coated with PDMS. The channel formed was 300 microns in length and 70 microns in width. The channel is shown in Figure 7.

In summary, in Chapter 2, the properties and advantages of SU-8 photoresist were discussed. The mechanism of electrochemiluminescence via annihilation and co-reactant is also described. Annihilation occurs by oxidative-reductive mechanism of ECL molecule whereas co-reactant occurs by introducing specie that would make the ECL molecule to undergo excited state. The excited state would hence return to ground state with the release of a photon. The generation of ECL by magnetic bead method and fabrication of microfluidic channel by three different techniques is referenced. The first technique of fabricating the channel involves forming metal electrodes by electroplating. Though the application of this channel was to pump and manipulate the flow of biological cells [19] it can also be used for testing ECL by applying a suitable voltage across the electrodes. In the second technique, indium tin-oxide electrodes were fabricated on a glass slide and the channel formed was sealed by a slab of PDMS. In the third technique, an epoxy substrate with a working and reference electrode was used to form the microchannel. The technique of fabricating microchannel used in this project requires only one photoresist as compared to two photoresists in forming vertical metal electrodes, a single lithography and metal evaporation step as compared to several processing steps which were required in forming indium tin oxide electrodes, and several inter-digitated arrays of fins thus, increasing overall sensitivity as compared to only two electrodes used in PCB method.

Chapter 3

Experimental Procedures

3.1 Fabrication Steps

The microfluidic channel for this project was formed by spin coating, soft bake, contact lithography, post exposure bake, development of resist and finally metal evaporation. All of the mentioned procedures were performed in clean room at the University of Houston's Nanofabrication Facility.

3.1.1 Spin Coating

Figure 8. Spin coater in clean room.

A spin coater, shown in Figure 8, is used to coat the substrate with a layer of photoresist. The substrate to be coated with the resist is placed on the vacuum chuck in the spin coater. The substrate used is a single-side polished silicon substrate with an oxide layer of up to 500 nm and

the photoresist used is SU-8 2050. A small amount of photoresist is generally dispersed on the center of the substrate. The spin coat parameters for achieving 50 micron thick resist as provided by Microchem Corporation (Newton, Massachusetts) are 10 seconds with a speed of 300 rpm and the acceleration being 100 rpm/second followed by 30 seconds with a speed of 3000 rpm with the acceleration being 500 rpm/second [22]. Two spin speeds are required to coat the substrate: the first evenly spreads the resist on the substrate to cover the entire surface at a low spin speed, while the second, coats the substrate with the resist to the desired thickness at a higher speed. This is achieved by action of centrifugal force on the liquid viscous photoresist while it is spun together with the substrate. The thickness of the resist depends on the viscosity of the resist, spin speed, acceleration, and temperature of the resist. The rate of drying of the film depends on temperature and humidity conditions surrounding the substrate. The thickness of the resist coated on the substrate is inversely proportional to the spin speed. Thus, for higher thicknesses of the resist a lower speed is required whereas for a lower thickness a higher spin speed is required [23]. After spin coating with the mentioned parameters, a uniform layer of 50 micron thick resist is coated on the substrate as seen in Figure 9. The substrate is then removed from the spin coater and placed on the hot plate to dry the wet resist.

Figure 9. Resist evenly coated on the substrate after spin coating.

3.1.2 Pre-exposure Bake

Pre-exposure or soft bake step is performed to evaporate the solvent from the resist. This is done to dry the resist and the substrate can be used for contact lithography. The bake step is

performed at two different temperatures. The resist is first heated from room temperature to an intermediate temperature of 65 ℃ and then to a final temperature of 95 ℃ [22]. The intermediate heating at 65 ℃ is required so that the resist does not experience immense stress while it is being heated from room temperature to a very high temperature at 95 ℃. The baking is done at 65 ℃ for 3 minutes and then at 95 ℃ for another 20-25 minutes. The time for heating the resist at 95 ℃ was found by experimentation. Since the resist is 50 micron tall, it requires longer baking time [5]. Once the baking has been performed, the temperature on the hot plate is then ramped down from 95 ℃ to 65 ℃ so that the resist does not experience stress during rapid cooling [24]. The substrate is then removed from the hot plate and is exposed to room temperature.

3.1.3 Contact Lithography

Figure 10. The mask aligner that was used in this work.

Lithography is a type of pattern transfer technique widely used in semiconductor industry. Types of lithography currently used are optical lithography, electron beam lithography, x-ray lithography, nano-imprint lithography, etc. The type of lithography used in this project to fabricate microchannels is contact lithography, which is a type of optical lithography. In optical

lithography, an ultraviolet light source is used to expose the photo-sensitive resist [25]. The term contact lithography in itself explains that the mask is in complete contact with the wafer. The mask used in contact lithography contains a pattern of the structure to be formed. It consists of transparent as well as opaque regions. The mask needs to be very clean since any dirt present on the mask may come into direct contact with the substrate and hence contaminate it. Also, a dirt particle will block light reaching the photoresist.

Contact lithography is performed using a mask aligner, and a photo of the Kasper printer used in this work is shown in Figure 10. The main components of the equipment are the light source, a collimating lens, a mask holder, a microscope positioner, and a substrate carrier [26]. The light source is a mercury vapor lamp, which generates light by an arc discharge. It emits wavelengths of light ranging from 185 nm to 600 nm with peaks at 365 nm and 400 nm. The light is then focused on the mask by a lens. The mask is attached to the equipment by taping it to a low–pass glass filter. Since the mask is in complete contact with the substrate, the light falls on the resist from the transparent regions of the mask, as seen in Figure 11. The opaque regions of the mask block the light. SU-8 has a very high optical transmission above 360 nm [22]. A low pass glass filter is used to allow wavelengths more than 360 nm thus passing i-line wavelength, which provides sharp features of the resist structure. It blocks wavelengths below 360 nm.

To expose the resist, the buttons for contact and expose mode are pressed on the equipment. An exposure time of 95 seconds is set on the equipment, after which the UV light turns off automatically. The photons from UV light activate a compound in the resist, which is known as photoactive compound or photoinitiator. The compound is so named since it activates on receiving photons and produces a small amount of acid. The time for exposure is decided after visually inspecting the structures obtained from the resist with several different exposure times. It is found that the exposure time of 95 seconds is sufficient to expose the top as well as the bottom part of the structure. Once the light turns off, the substrate is then removed from the equipment and a post exposure bake step is performed on the resist.

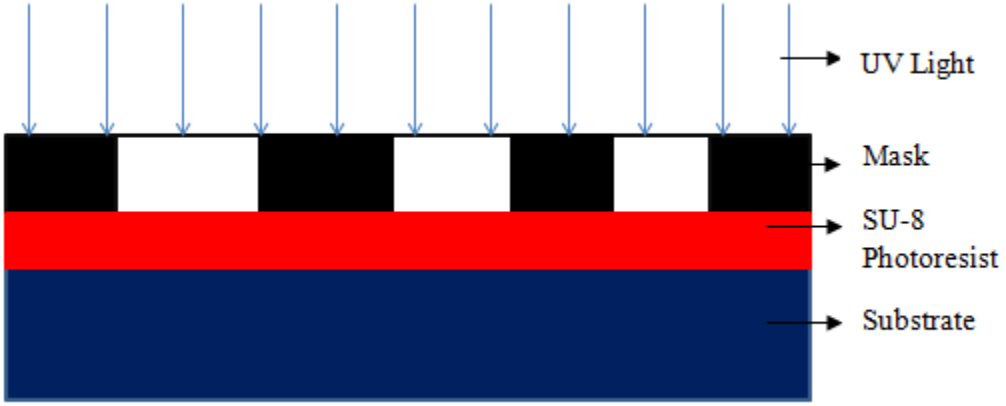

Figure 11. Exposure of resist to UV light. Transparent regions on the mask let light pass through it whereas opaque regions block light.

3.1.4 Post Exposure Bake

The post exposure bake step is also performed in two stages wherein the first step ramps the resist from room temperature to 65 ℃ for 1 minute and then to 95 ℃ for 6-7 minutes [22]. Since, SU-8 is a negative photoresist, the pattern of the channel appears on the resist in 5 seconds during its baking. The small amount of photoacid, which was released in the exposure step now acts as a catalyst and produces even more amount of acid. The acid produced cross-links the entire exposed structure to render it insoluble into the developer solution [27]. After the post exposure bake step, the substrate is placed in a beaker containing the developer to dissolve the uncross-linked resist.

3.1.5 Development

The developing step is performed by submerging the substrate in a solution of SU-8 developer. The development time for SU-8 2050 resist is 6-7 minutes. The unexposed regions of the resist dissolve into the developer solution whereas the exposed regions of the resist, which are cross-linked after the post exposure bake step, remain on the substrate, as seen in Figure 12. After development, the substrate is then treated with iso-propanol (IPA) and dried with nitrogen gas. A

white film may develop after rinsing with IPA, which indicates that the development is insufficient. To eliminate the film, the substrate is immersed in SU-8 developer again and rinsing step is performed till the white film disappears [22].

Figure 12. Exposed regions of the resist remain on the substrate whereas unexposed regions dissolve into the developer solution.

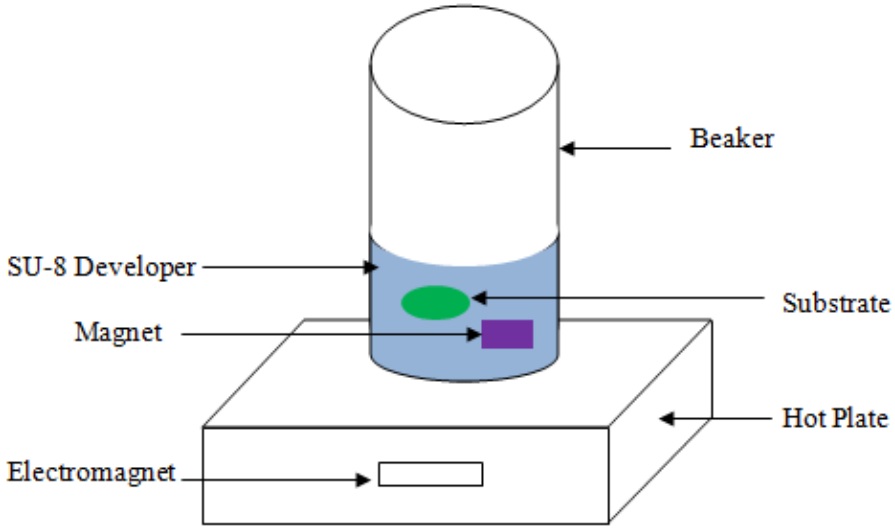

Figure 13. Development bath set-up consisting of a beaker, magnet, hot plate, substrate, and SU-8 developer.

In order to avoid manual stirring of the substrate in the developer solution for the designated development time, magnetic method of stirring was employed to reduce the labor and achieve more consistent results. In this method, a stir bar/magnet is placed in a beaker containing the developer solution and the substrate, as seen in Figure 13. The bar used was inert to the

developer solution and consists of a permanent magnet encapsulated in a Teflon coating. The beaker was then placed on a hot plate. The hot plate includes a rotating magnetic field and the speed of rotation on the plate was set to 250 rpm. The heating element in the hot plate was not used and the solution was held at room temperature. Thus, due to rotating magnetic field, the stir bar keeps on rotating. This in turn stirs the liquid and hence dissolves the unexposed regions on the substrate.

3.2 Lithography Mask

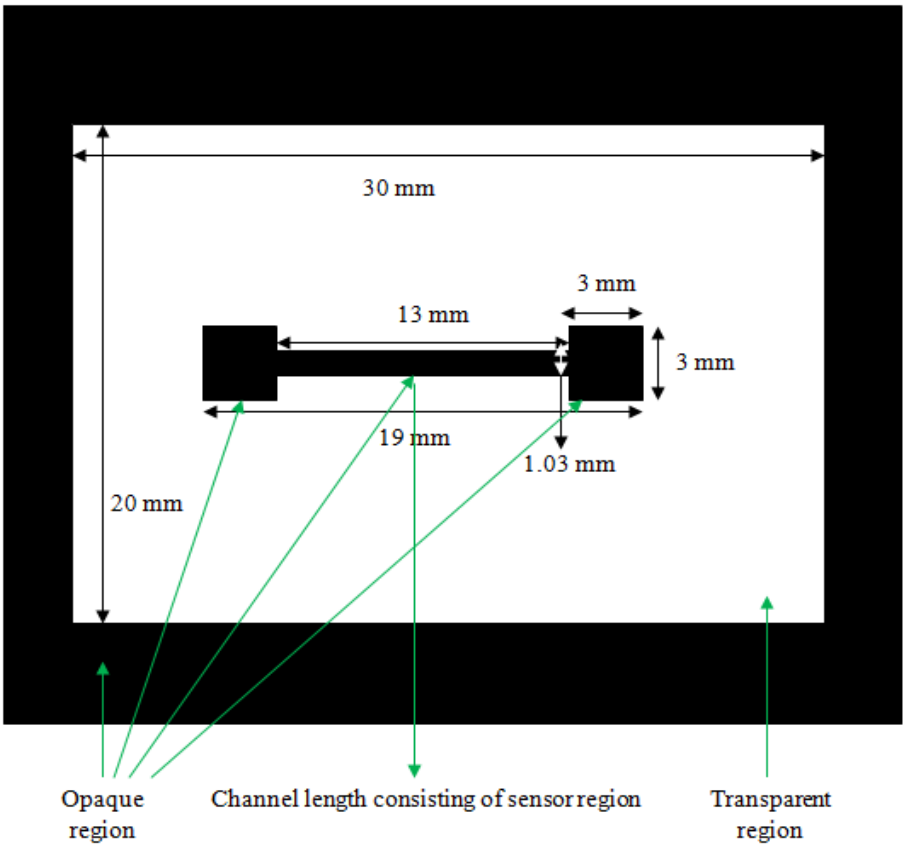

Figure 14. Dimensions of the microfluidic channel. The channel is 13 mm long, 1.03 mm wide, and consists two 3 mm ports.

A transparency mask printed by CAD/Art Services Company (Bandon, Oregon) and a filter glass from Omega Optical Inc. (Brattleboro, Vermont) [28] was used to support the

transparency mask on the mask aligner equipment. The mask dimensions are shown in Figure 14. The channel is 13 mm long, 1.03 mm wide and contains two 3 mm ports. Several fins were used in the structure so that in the event of the breakage of one fin; other fins could function effectively, thereby not adversely affecting the functionality of the device. The white region indicates that UV light will penetrate directly through it, thus exposing the photoresist (i.e. it is the transparent region). The exposed photoresist then cross-links in the post exposure bake step, forming a long polymer bar. The black regions, which are the opaque regions, block the light. Any photoresist in those regions will be washed away in the developer solution as it does not cross-link. The microfluidic mask shown in Figure 15 has an inter-digitated pattern to connect alternate bars in the pattern to either positive or negative electrode. Furthermore, the self-aligned feature of the pattern eliminated the need of any lithographic masks for coating the walls of the channel to form electrodes.

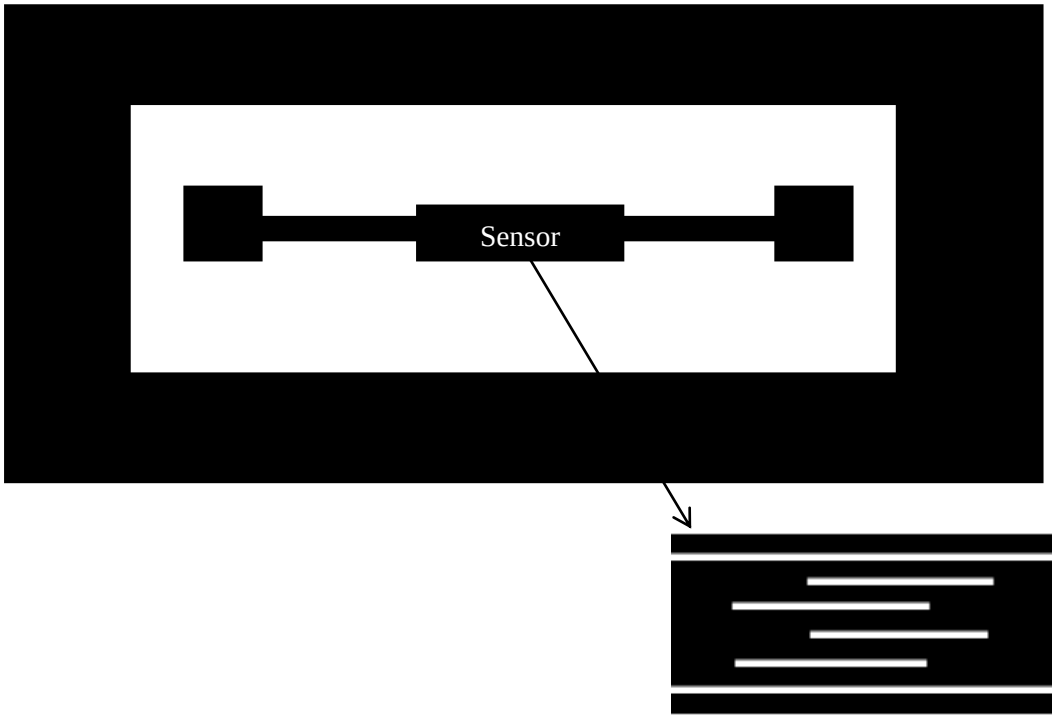

Figure 15. Lithographic mask showing the microfluidic channel. The sensor region consists an inter-digitated array of electrodes.

3.3 Angled Evaporation

Metal films are coated on a substrate by thin film deposition technique, which can be in the form of physical or chemical vapor deposition. The technique of forming thin films on the substrate used in this project is physical vapor deposition. In this process, a crucible containing the source material is heated inside a vacuum chamber until the vapor flux of the material is sufficiently high to allow for the deposition of the material at the wafer surface at sufficiently high rates. In particular, electron beam physical vapor deposition was used to coat the channel walls with metal.

The electron beam evaporator consists of a tungsten filament (the electron source), a substrate holder, crucibles to hold the source material, crystal rate monitor, focusing and deflecting magnets, and a high vacuum pump. The system that was used for this work is shown schematically in Figure 16. A tungsten filament is heated below a carousel that houses the evaporation source material until it emits a large electron current. The electrons are accelerated and focused to a small spot on the source material [29] housed in the crucible, which is located at the opposite side of the electron source so that any evaporated tungsten cannot contaminate the wafer. The system is pumped by a compressed helium cryogenic pump and reaches a base pressure of 6×10^{-6} Torr after pumping for 10 minutes. The electron beam heats the source material, causing it to melt or sublime. Thus, the metal vaporizes and travels to the substrate where it condenses to form a thin film.

The crystal rate monitor provides the rate of film being evaporated and hence the thickness of the film being deposited. It consists of a vibrating crystal whose natural frequency shifts as material deposits on its surface. The change in natural frequency indicates the amount of deposited material. The electron beam evaporator in the clean room at University of Houston has a chamber allowing the user to tilt the substrate relative to the source.

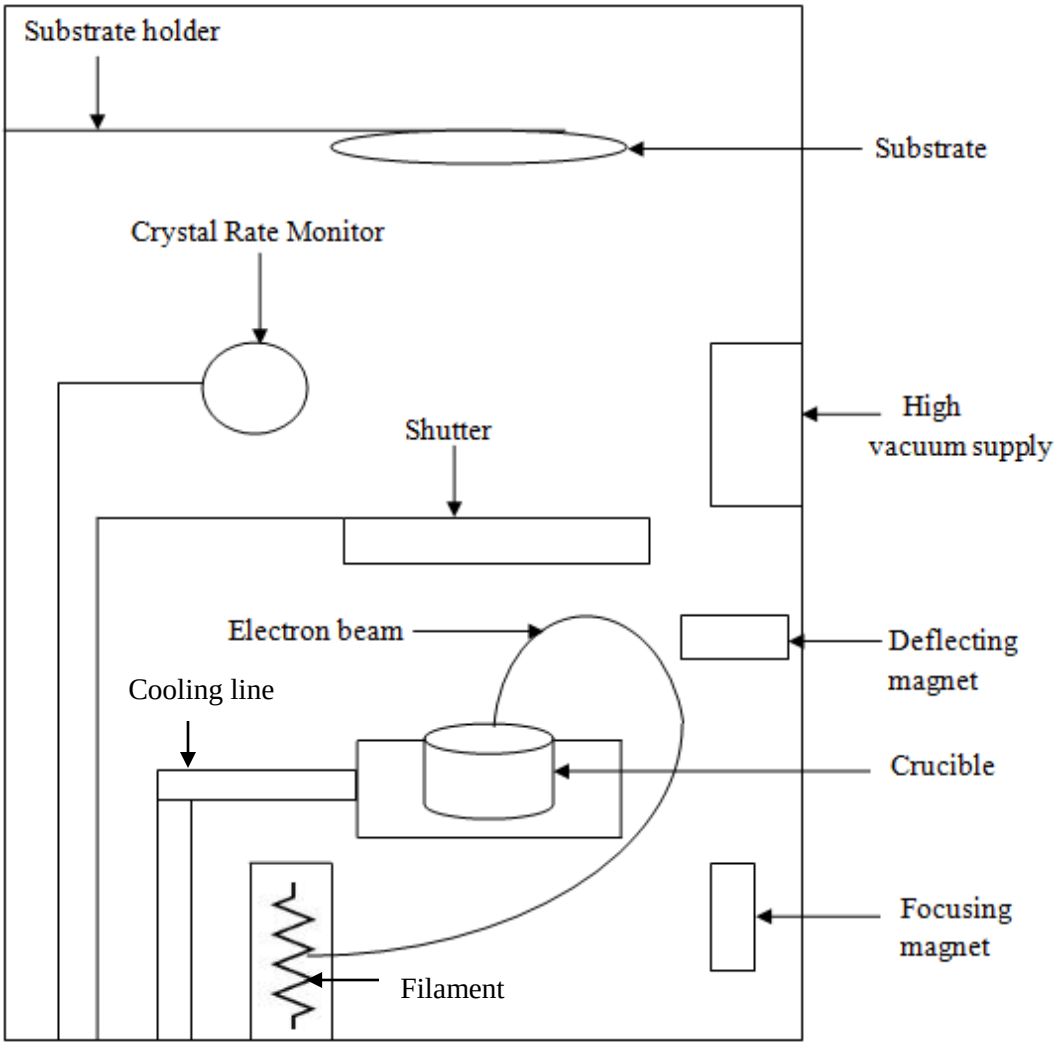

Figure 16. Schematic of electron beam evaporator.

To form electrodes, the polymer had to be coated with a metal. Care had to be taken during coating so that there would be no metal between adjacent fins as that would short the structure as shown in Figure 17 (a). Thus, the angle of arrival of the metal was adjusted to coat the polymer to a certain depth without coating its base as shown in Figure 17 (b). The walls would then be connected alternately to positive or negative electrode by an additional step of metal coating. The electron beam evaporator used for this project is shown in Figure 18.

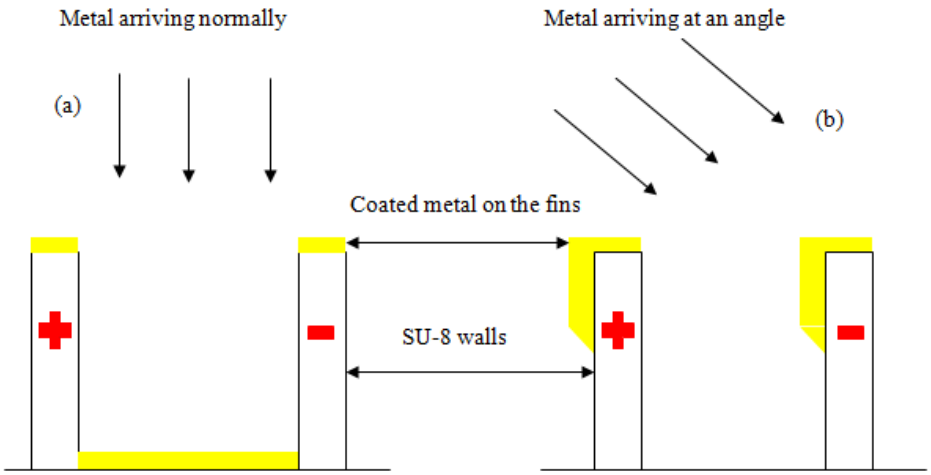

Figure 17. Metal coated on the SU-8 walls. (a) Metal arriving normally shorts the structure. (b) Metal arriving at an angle coats only the top of the polymer and it is ensured that there is no metal connecting the two electrodes.

Figure 18. The electron beam evaporator equipment in the clean room.

The metal used for evaporation was chromium. Although there is flexibility in the choice of metals that can be used for forming electrodes, chromium was used in this project as it required

low current of 50-70 mA to evaporate it, had high rates of evaporation (2 nm/sec), did not have a tendency to oxidize quickly when compared to copper and aluminum, was cost-effective, and was fully optimized on the existing equipment. If other metal coatings are desired, these can be deposited by changing the source material in the evaporator. The choice of metal is ultimately determined by the needs of the ECL process.

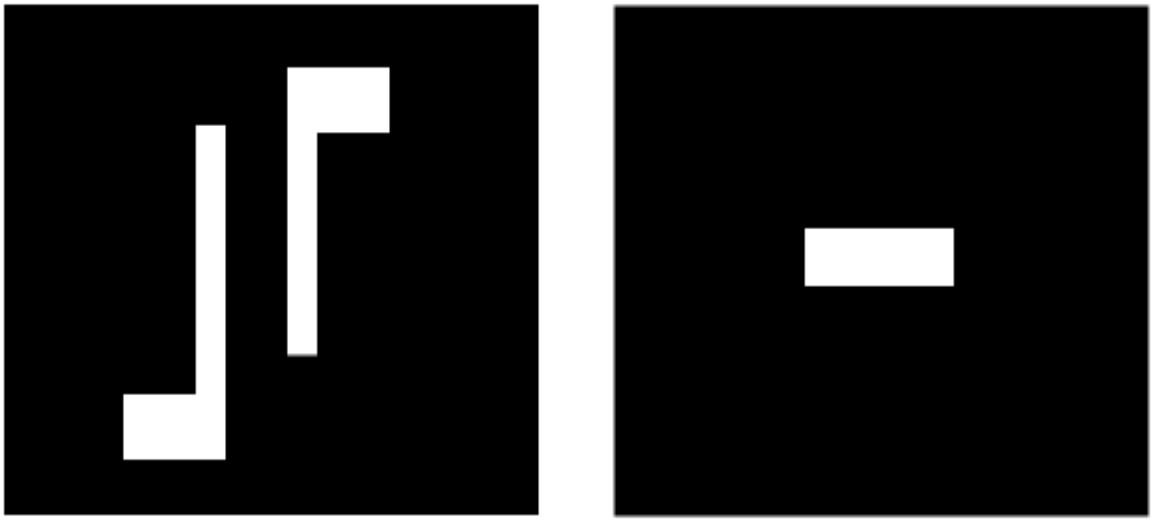

(a) **(b)**

Figure 19. The two types of stencil used in this work: (a) the stencil used for forming electrodes and (b) the stencil used for coating channel walls.

.

In order to form electrodes, two masks were required. The mask in Figure 19 (a) was used to connect alternate fins whereas the mask in Figure (b) was used to coat the channel walls. The stencils were cut from Aluminum shim stock by a rapid prototype digital craft cutter, similar to the one in reference [30]. The white region on the mask is a cut made in the shim stock so that metal can pass through the open region and hence coat the channel walls. The black region on the mask is the closed region and hence it blocks any metal to pass through it. In Figure 19 (a), the two 'L' shaped electrodes are placed 3.5 mm apart. Figure 20 shows the device structure obtained after coating with metal.

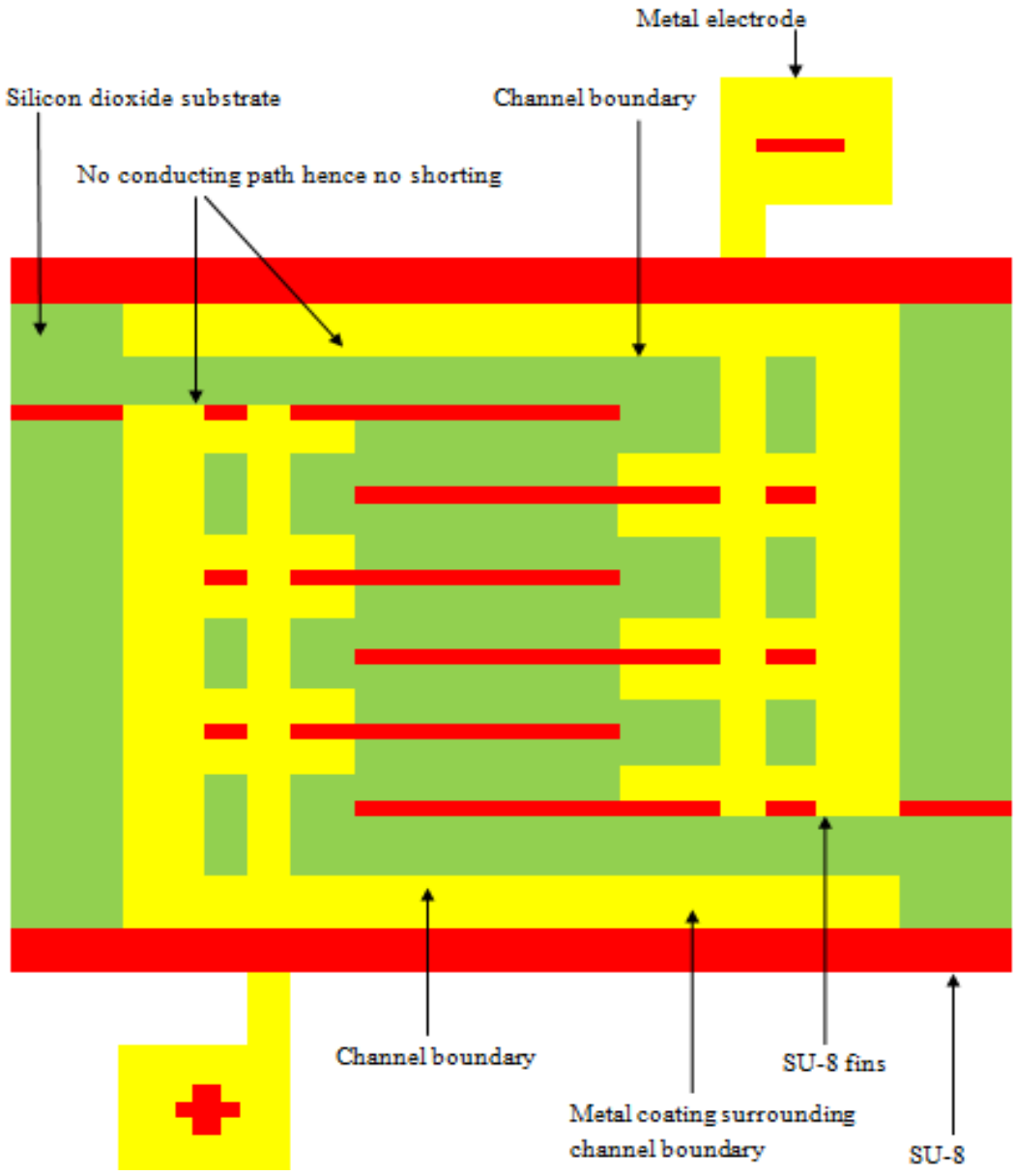

Figure 20. Final structure of microfluidic device after coating metal using double-angled evaporation technique on SU-8 walls to form electrodes.

The angle of substrate tilt is calculated by taking the tangent of distance up to which the shadow is cast (60 microns) divided by the height of the resist (50 microns). For electrode formation, the angle was found to be $\Theta = \tan^{-1}(60/50) = \sim 50^0$. For coating channel walls, the angle was found to be $\Theta = \tan^{-1}(80/50) = \sim 60^0$.

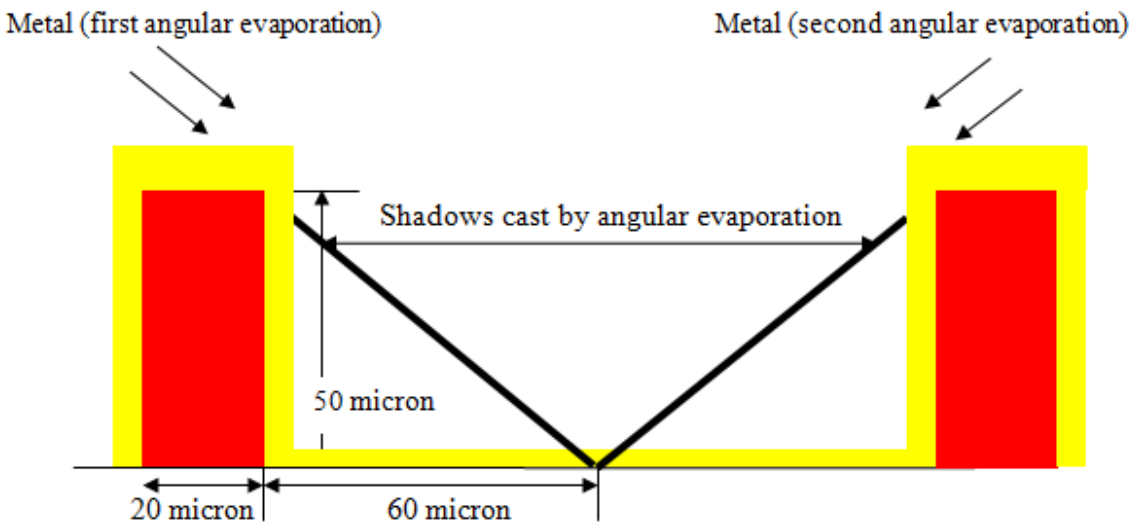

Figure 21. Shadows cast by walls due to tilting of substrate on both sides at an angle.

Since, the angle for metal coating should be more than the spacing between the two adjacent fins which is 50 microns and the width of fins which is 20 microns; the angle in the evaporator was set so that the fins will cast a shadow greater than 70 microns. Since, the SU-8 wall is 50 micron tall and fins are spaced 50 microns apart, a 45^0 angle would hence cast a shadow up to 50 microns. Similarly, a 55^0 angle will cast a shadow up to 70 microns and a 67^0 angle will cast a shadow up to 120 microns which is also the total distance between two alternate fins. Hence, the angle used to form L-shaped electrodes was 50^0 and for casting channel wall shadows the angle selected was 60^0.

The selection of angles to cast shadows is flexible however the above mentioned angles were selected to assure that no shorting occurs between the fins. A 50^0 angle would make a 50 micron tall SU-8 structure to cast a shadow up to 60 microns, as seen in Figure 21. This insures that the long bar at the end, its consecutive fin and the boundary of the channel are not connected. A lower angle can be selected for forming electrodes since the fins in the sensor region are masked by the evaporation mask and hence they do not receive metal. A 60^0 angle would cast a shadow up to 80 microns thus preventing shorting between the adjacent fins, as seen in Figure 22.

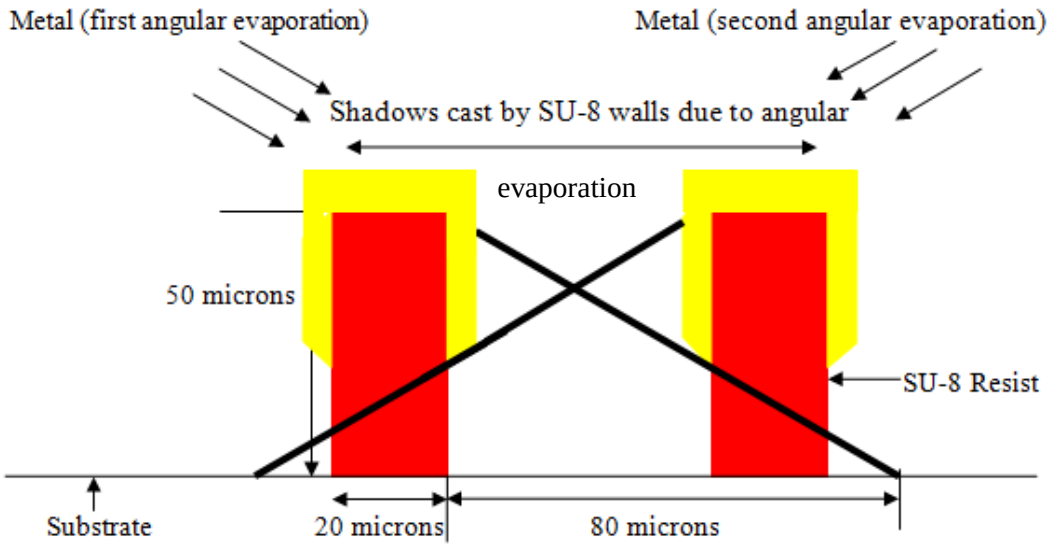

Figure 22. Shadows cast by SU-8 walls is up to 80 microns.

The entire fabrication sequence for fabricating microchannel and forming electrodes is summarized in Figure 23. The microchannel can then be used for electrical measurements.

(a) First, a silicon dioxide substrate is coated with 50 microns thick SU-8 photoresist. The substrate is placed on a hot plate at temperatures of 65 ℃ and 95 ℃ for durations of 3 and 25 minutes respectively to evaporate the solvent from the resist. Once the substrate is dried, it is then placed in mask aligner.

(b) A transparency mask with the microfluidic pattern was taped to the optical filter and placed on top of the substrate. An exposure time of 95 seconds was used to print the pattern. After exposure to UV light for the designated time, the substrate was removed from the equipment and placed on a hot plate at 95 ℃ for duration of 7 minutes to complete the post-exposure bake step.

(c) The substrate is developed so that the un-cross linked regions dissolve in the developer and the cross-linked regions remain on the substrate. The substrate was then rinsed in IPA and dried with nitrogen gas to form the microfluidic channel.

(d) To coat the channel walls with metal, double-angled evaporation technique was used in an electron beam evaporator. The angles set in the evaporator equipment for forming

electrodes and coating channel walls were 50^0 and 60^0 respectively. The metal coated on the channel walls was 150 nm whereas metal on the base was 300 nm. There was no metal within the spacing between adjacent walls.

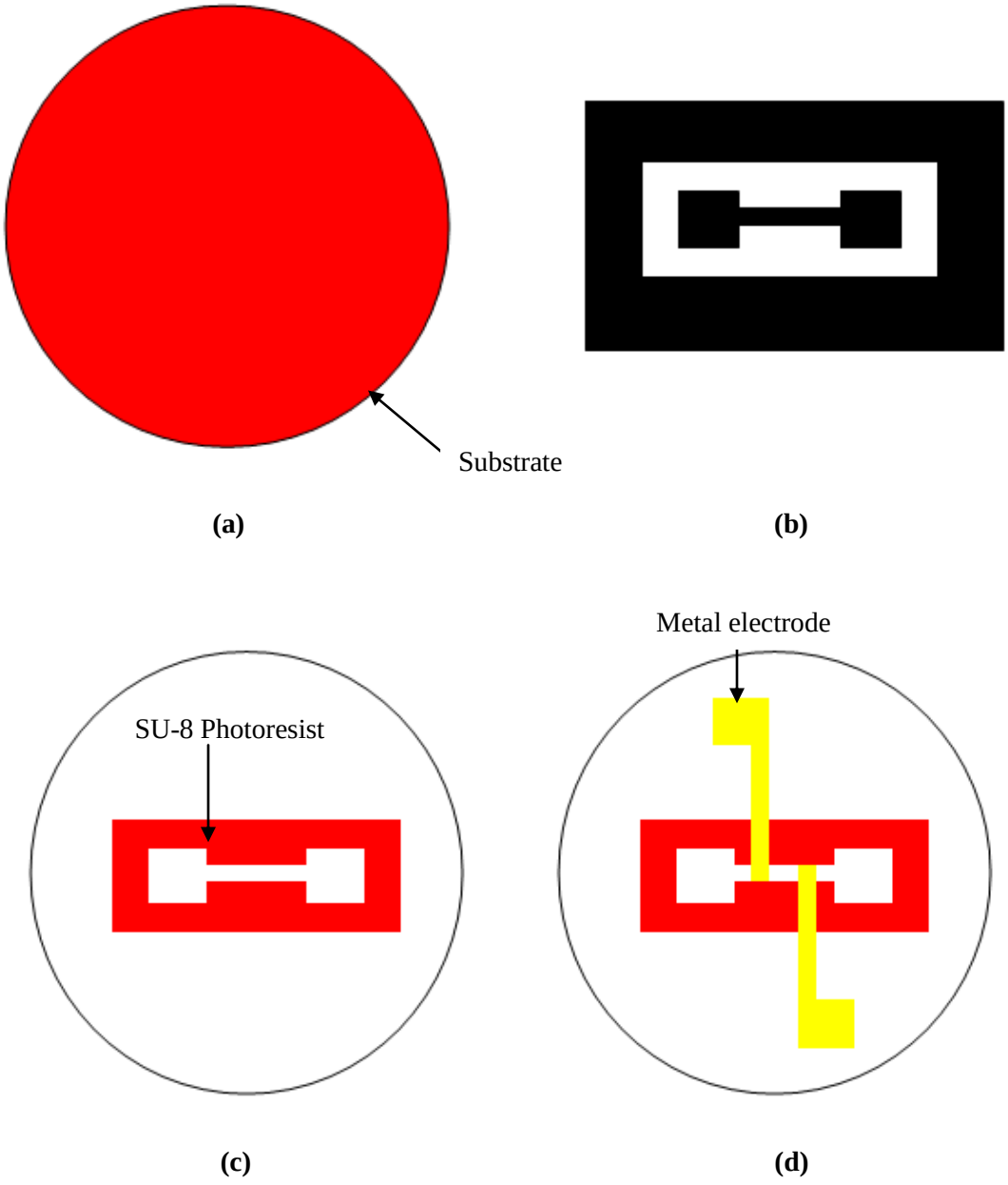

Figure 23. Entire fabrication sequence for forming microfluidic channel. (a) Substrate is coated with SU-8 photoresist. (b) Lithographic mask consisting of inlet and outlet port along with the channel. (c) Pattern obtained on the substrate after contact lithography and development. (d) Electrodes are formed via double-angled evaporation technique.

3.4 Measuring Resistance

In order to determine that the structures work as expected, the resistance of the channel was measured by placing the ohm-meter probes across the two ends of the metal plates without having any solution dispersed in the channel. Two solutions of known resistivity, DI water and PBS (Phosphate Buffered Saline) solution were then dispersed in the channel and their resistance is measured. The obtained resistance from the ohm-meter is compared with the calculated resistance. The resistance was calculated by using standard values of resistivity for the two solutions and channel dimensions. Figure 24 shows the microfluidic channel obtained after forming electrodes. It consists of two ports, two long 'L' shaped metal electrodes, and cross-linked SU-8 2050 resist that defines the boundary of the channel. Figure 25 shows the ohm-meter connections to measure the resistance of the liquid in the channel. Two probes of the ohm-meter are connected to the two 'L' shaped electrodes.

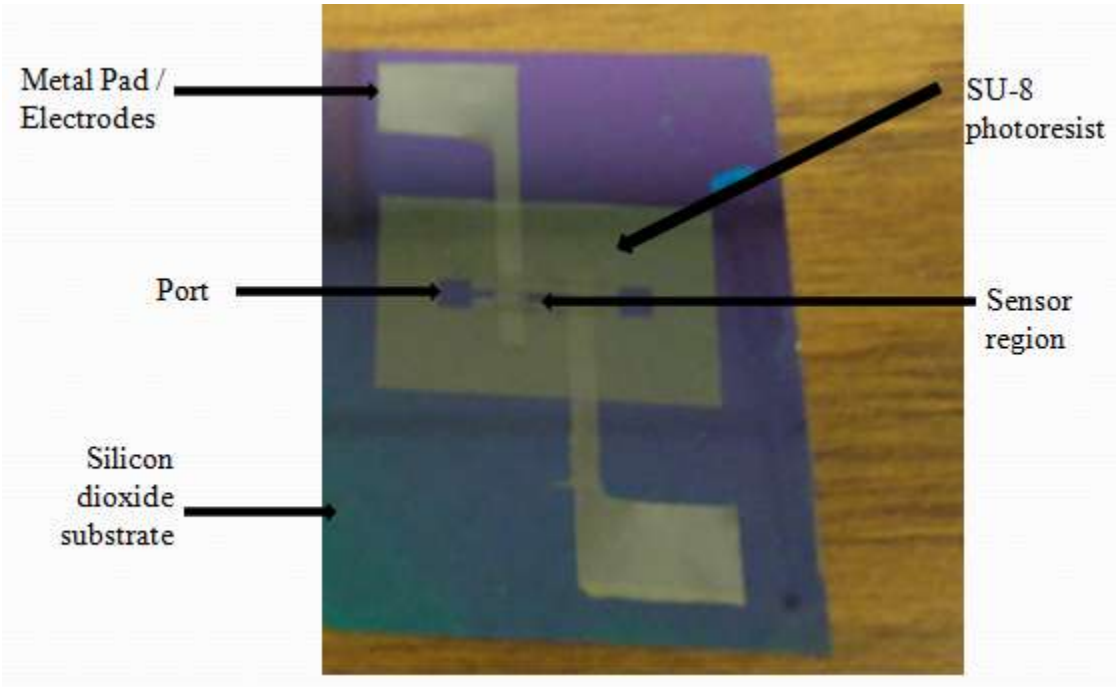

Figure 24. Microfluidic channel on silicon dioxide substrate with SU-8 channel walls and chromium metal electrodes.

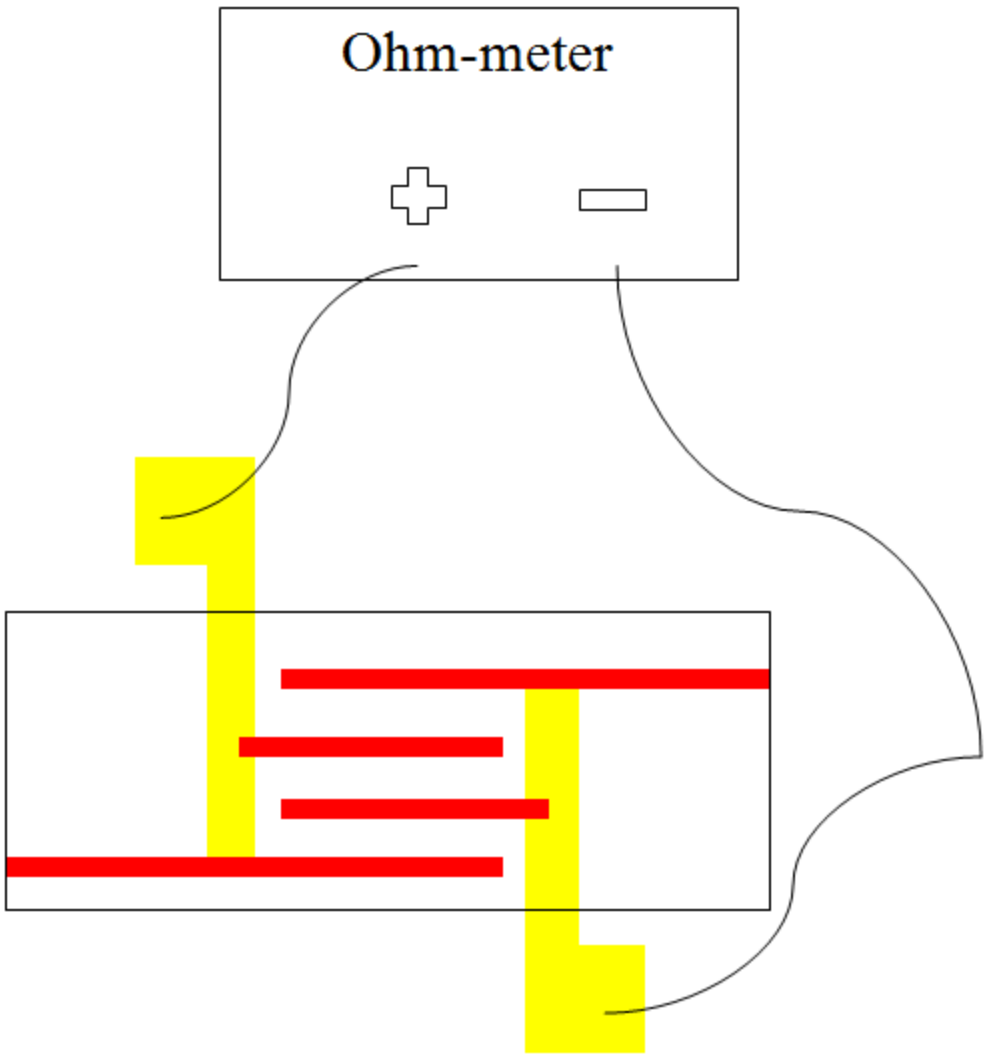

Figure 25. Ohm-meter probes are connected across the electrodes to measure resistance of liquid in the channel.

Chapter 4

Results and Discussions

4.1 Optimizing Exposure Dose

Figure 26 shows that the SU-8 pillars have toppled on each other. The process parameters used were described in Section 3.1. The pillars have a 10 micron feature size and are spaced apart by 10 micron. The toppling of the structures occurred due to under-exposure as the top part of the resist got exposed completely whereas the bottom part did not receive sufficient light to cross-link. Thus, during development, the developer etches laterally at the under-exposed regions, forming a nail-like structure. Longer exposure times are needed in order to determine the best exposure dose for the 50 micron tall SU-8 structure.

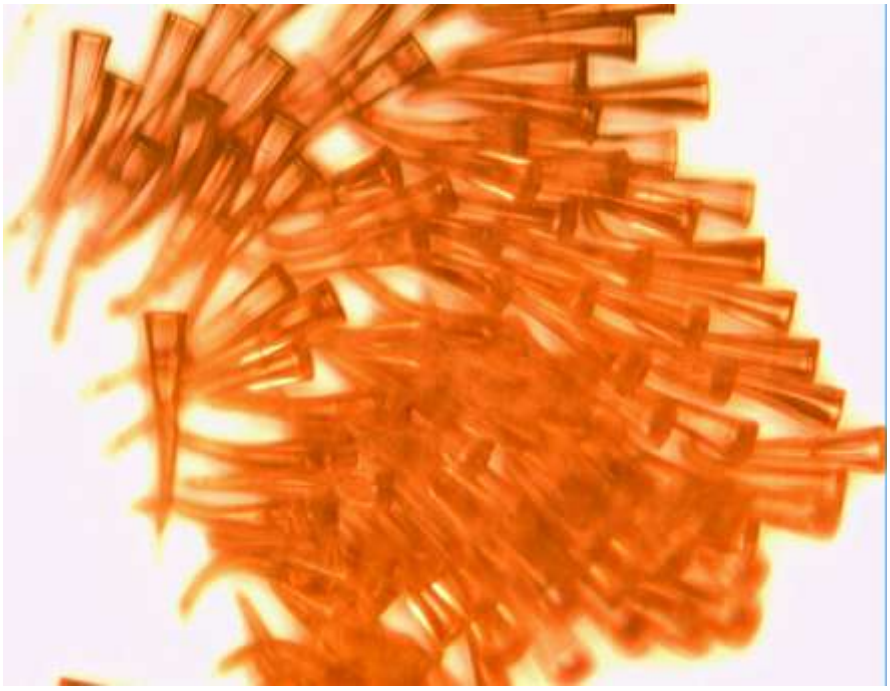

Figure 26. Due to under-exposure, the 50 micron tall pillars have toppled over each other.

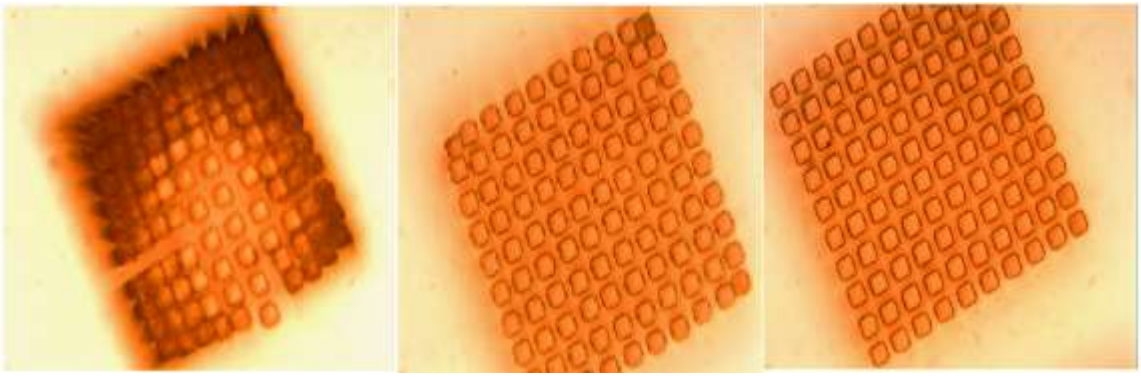

(a) **(b)** **(c)**

Figure 27. On increasing the exposure time the probability of light reaching the base of the 50 micron tall pillars also increases, which eliminates issues like toppling and collapsing of walls due to a much stronger base. (a) 45 seconds exposure. (b) 60 seconds exposure. (c) 75 seconds exposure.

In Figure 27, we see that on increasing exposure time, the sharpness of the walls also improves. The squares in Figure 27 (a) are misaligned as well as distorted whereas the squares in Figure 27 (c) have comparatively sharp edges. However, the base of the resist remains weak even at 75 seconds of exposure since the 50 micron tall pillar were found to break while doing profilometry. Thus, it is concluded that exposure times of 75 seconds or below is insufficient to expose a 50 micron thick photoresist. Hence, in the next set of experiments carried out, an exposure time of 90 seconds or higher was used to expose the photoresist.

4.2 Stress

Figure 28 shows stress issues like buckling and sticking of polymer bars. The process parameters as discussed in Section 3.1, the microfluidic mask, and a snap spin step were utilized to carry out the experiment. In snap spin step, along with the two spin speeds a final spin step is performed for five seconds at 6000 rpm to drive off the excess resist accumulated on the edges of the substrate. The figure shows a wavy polymer wall resembling buckling of a string. The

polymer wall turns wavy due to compressive stress. There can be several reasons for stress that was experienced by the channel walls. Firstly, it could be because of the dimensions of the microfluidic pattern. The channel walls swell in development stage since [31], the molecular weight of the resist increases as it cross-links. Due to swelling of channel walls, the 15 micron spacing between adjacent walls reduces; hence causing sticking of adjacent walls. Secondly, it could be due to insufficient drying of the resist. Thirdly, the stress can be due to snap spin step, which causes the polymer molecules to vibrate at a very high speed of 6000 rpm, thus, inducing stress. Moreover, it can be because of rapid heating and cooling of the resist. The soft bake step is a stress inducing step because the polymer film is heated from its room temperature to a high temperature of 95 ℃ in a short span of time. Hence, there is rapid heating, which causes stress. The post exposure bake step can also induce stress as the polymer is again heated from room temperature to 95 ℃. Increasing exposure dose did not solve the stress issue as the cracking and buckling of walls was observed at all higher exposure times.

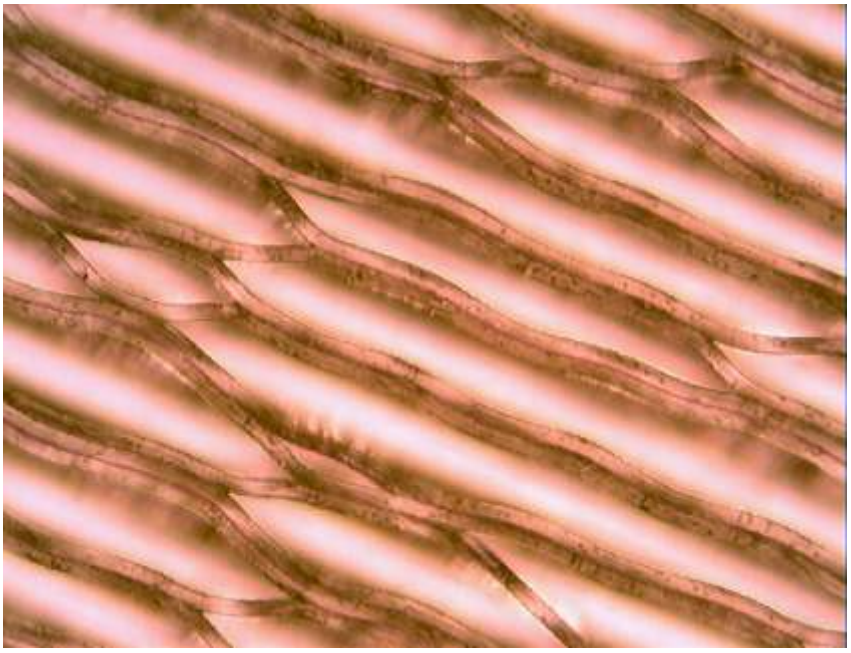

Figure 28. Stress within polymer that causes buckling, sticking, and delamination of walls in the channel.

4.3 Determining Cause of Stress

4.3.1 Thickness of Resist

In order to determine if higher thickness of the resist i.e. 50 microns causes stress, a lower thickness of 5 microns was used with the same microfluidic mask. The process parameters were utilized as provided by Microchem Corporation. The spin coating parameters were 500 rpm for 10 seconds and 2000 rpm for 30 seconds. This was followed by a soft bake at 95 ℃ for three minutes. A two step soft bake was not required since; a lower order thickness of the resist was used. The photoresist was then exposed to UV light for 90 seconds. A post exposure bake step was performed at 95 ℃ for 3 minutes to cross-link the exposed structure. After post exposure bake, the substrate was agitated in SU-8 developer for a minute and rinsed with IPA. It was dried with nitrogen gas [32].

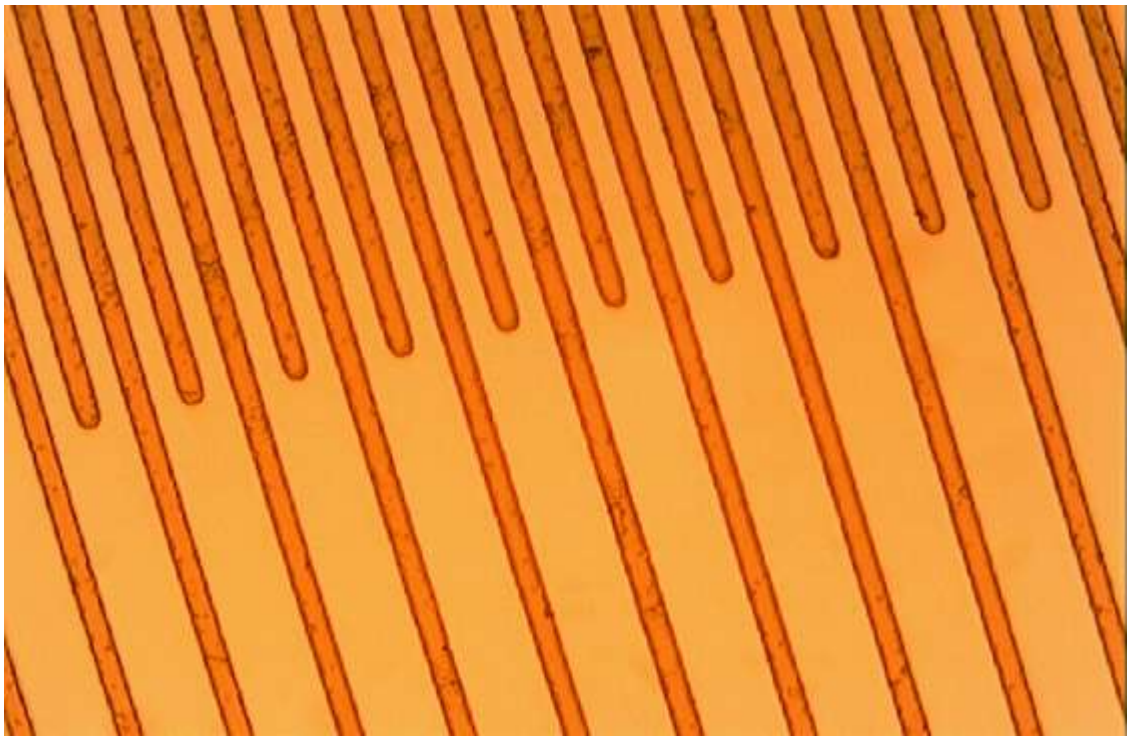

Figure 29. Inter-digitated array of polymer walls fabricated using SU-8 2005 resist. The walls formed are devoid of any stress effects due to lower aspect ratio of structures.

As seen from Figure 29, there are no stress issues like buckling and cracking of the walls. Since, the walls were 5 microns thick and 10 microns wide, the aspect ratio for them is 2:1. The long polymer bar has a wider base to stand and it can hence withstand all the rigorous processing steps. However, this is not the scenario with SU-8 2050, as the height of resist is five times more than the width of the walls thus, providing a thin base for the polymer to withstand all the processing steps. This shows with higher aspect ratio, there is high amount of stress within the polymer.

4.3.2 Process Parameters

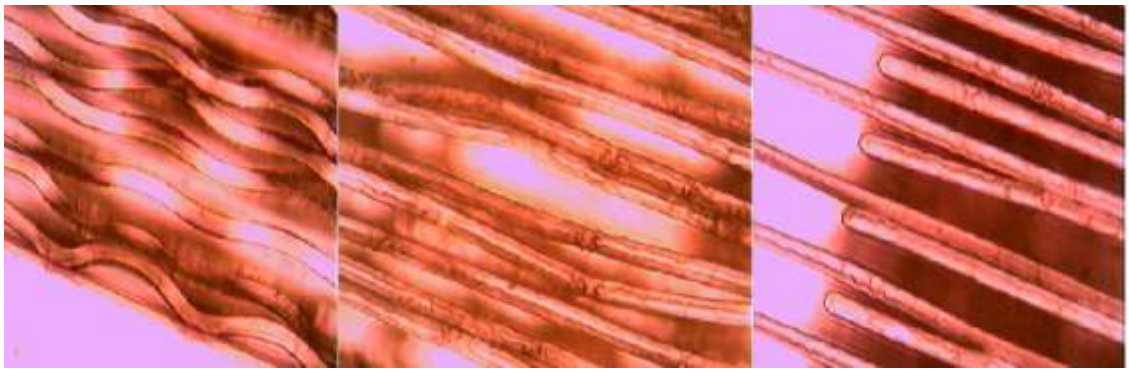

(a) **(b)** **(c)**

Figure 30. Stress issues such as buckling and de-lamination of walls are observed with all the processing steps. (a) Snap spin and two-step soft bake. (b) Normal spin and one-step soft bake. (c) Normal spin and two-step soft bake.

The process parameters were changed one at a time to determine if stress was caused due to any particular processing step. As seen in Figure 30, there is buckling, sticking, and de-lamination of walls.

(a) In snap spin and two-step soft-bake, it is seen that there is buckling of walls. With snap spin, as the molecules of the polymer vibrate at a very high speed, they experience immense

vibration and collide with the adjacent molecules. A two-step soft bake is unable to eliminate stress as the polymer has already experienced immense stress due to snap spin.

(b) In normal spin and one-step soft bake, the walls drifted from their original position. This was due to rapid heating of the polymer from room temperature to a very high temperature of 95 ℃.

(c) In normal spin and two-step soft bake, it is observed that the walls have buckled. Moreover, the developer solution was not able to reach the bottom of the 50 micron tall structure due to the limited spacing between the adjacent walls. Stress in the resist was also due to poor adhesion of resist to the substrate which caused de-lamination of the polymer walls as seen in the figure. The recipe of normal spin and two-step ramping should have provided a fine pattern as expected however, as all the steps discussed above failed to eliminate stress experienced by the polymer during the processing steps, it was hence decided to change the dimensions of the channel.

4.4 Changing Dimensions to Eliminate Stress

The next lithography mask that was designed had two patterns. In the first pattern, the width of the walls was unchanged and spacing between adjacent walls was increased to 50 microns. For the second pattern, the width of walls was increased by 10 microns thus, the final width being 20 microns. The spacing between the alternate bars for the two patterns was increased to 50 microns in the new mask to assure that the developer solution will be able to reach the bottom of the structure and remove the un-cross linked polymer. The dimensions in the first pattern were selected to test if increasing spacing between adjacent walls by keeping the width same would eliminate the sticking of adjacent fins. In the second pattern, the width of the fins was increased by 10 microns to test if increasing the width would eliminate buckling of the

walls as that gives the polymer a wider base to stand. Since, it was also found that, there is incomplete drying of the resist; the baking time was increased from 9 minutes to 25-30 minutes.

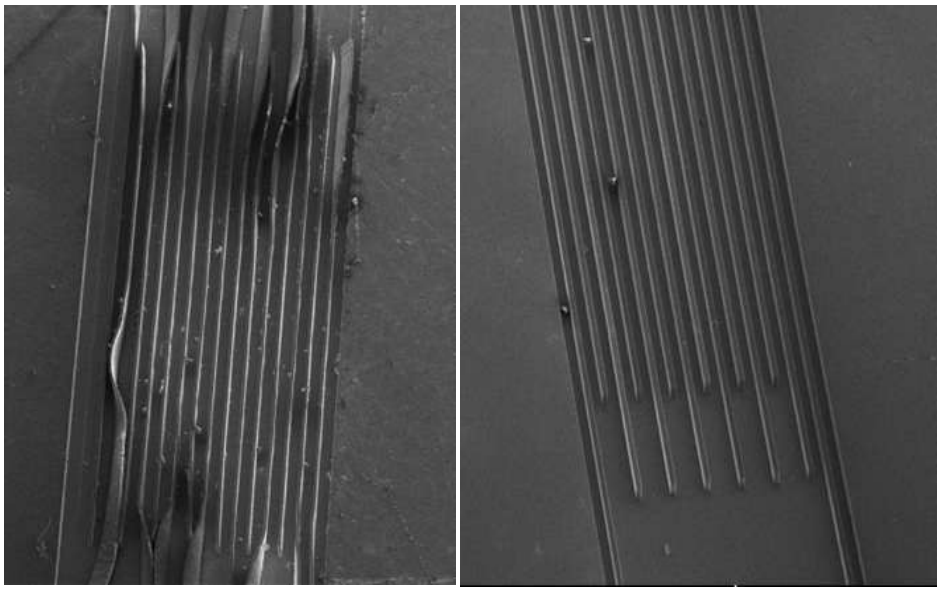

(a) **(b)**

Figure 31. SEM image of microfluidic channel with 50 microns spacing between adjacent walls. (a) With 10 microns width of walls, the polymer has a small base to stand hence, it has buckled and cracked. (b) With 20 microns width of walls, the polymer has a wider base to stand hence, the walls formed are straight.

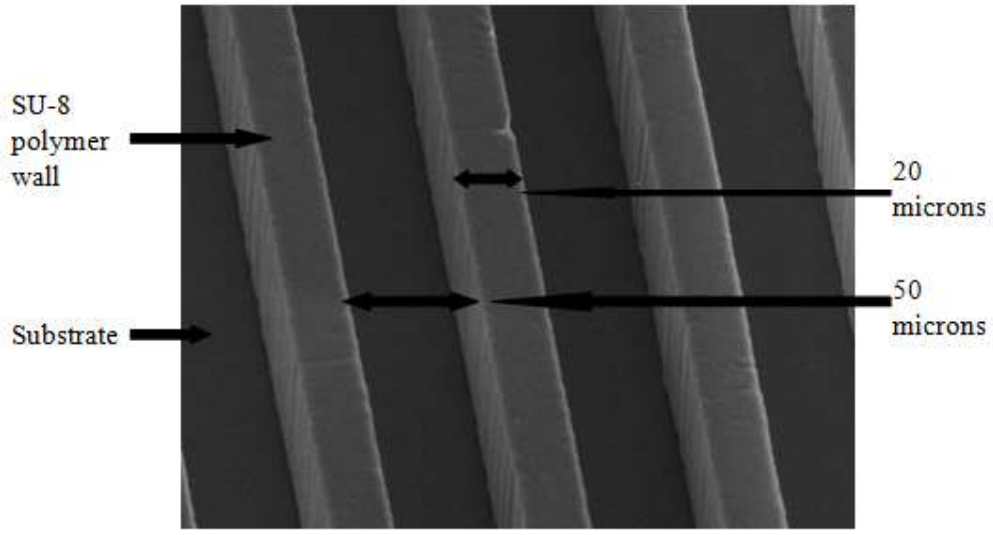

Figure 32. SEM image of SU-8 walls showing the long polymer bars.

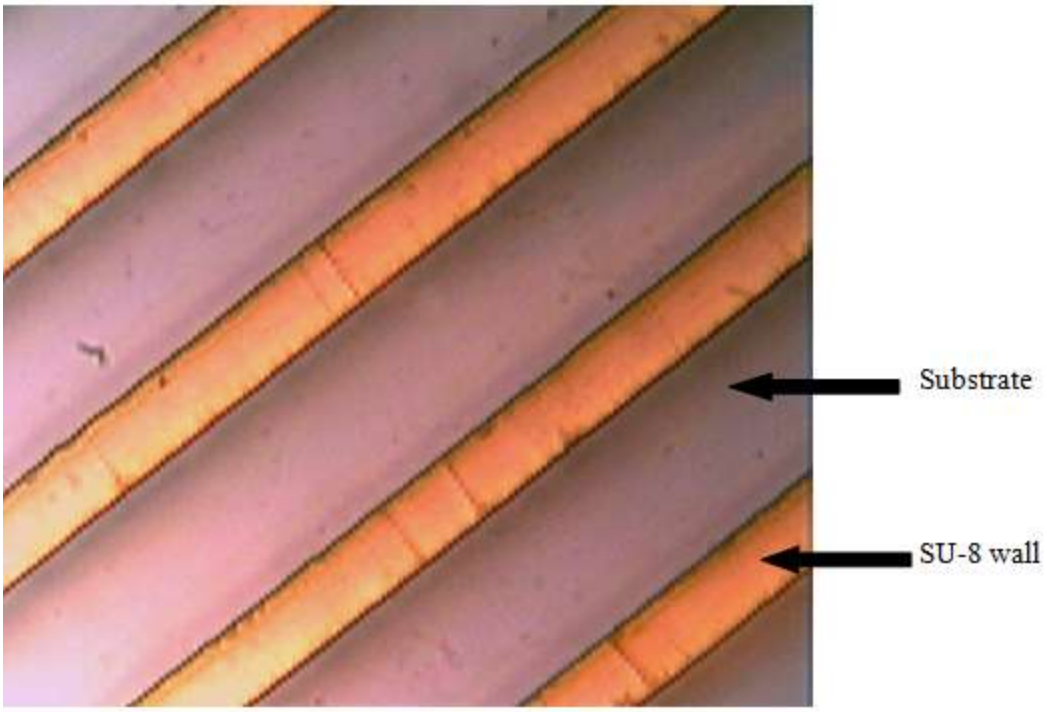

Figure 33. Optical Microscope image of SU-8 walls formed on the substrate.

The walls in Figure 31 (a), are 10 microns wide and the spacing between the adjacent walls is 50 microns. As seen in the figure, the walls appear very thin. Also there are issues such as poor adhesion of polymer to substrate, buckling, and cracking of walls. Several particles of polymer are stuck on the walls which can cause obstruction to the flow of fluid. Hence, it was decided to discard the dimension for 10 microns width of walls. The walls obtained appear straight in Figure 31 (b) and there is no buckling or sticking of walls. Hence, from analyzing the images, it was deduced that the combination of 20 microns width of walls and 50 microns thickness certainly serves the best and was finalized as the channel wall dimensions. Figure 32 and 33 shows the SEM and optical microscope image respectively of the walls which confirm that the stress issues have been eliminated after changing channel dimensions. Furthermore, with increased baking time the sample dries rapidly and hence the further experiments performed were with a baking time of 25 minutes.

4.5 Shorting of Electrodes

There was shorting issue due to the two long polymer bars at the two ends of the channel as seen in Figure 34. Thus, the positive and negative electrodes are connected to each other which shorts the entire structure. Initially an electrical break was decided to be introduced in the channel to prevent shorting. However, that would obstruct the flow of fluid. It was then decided to shorten the end bars to a limit where they would align with their alternate fins and hence be connected to either the positive or negative electrode.

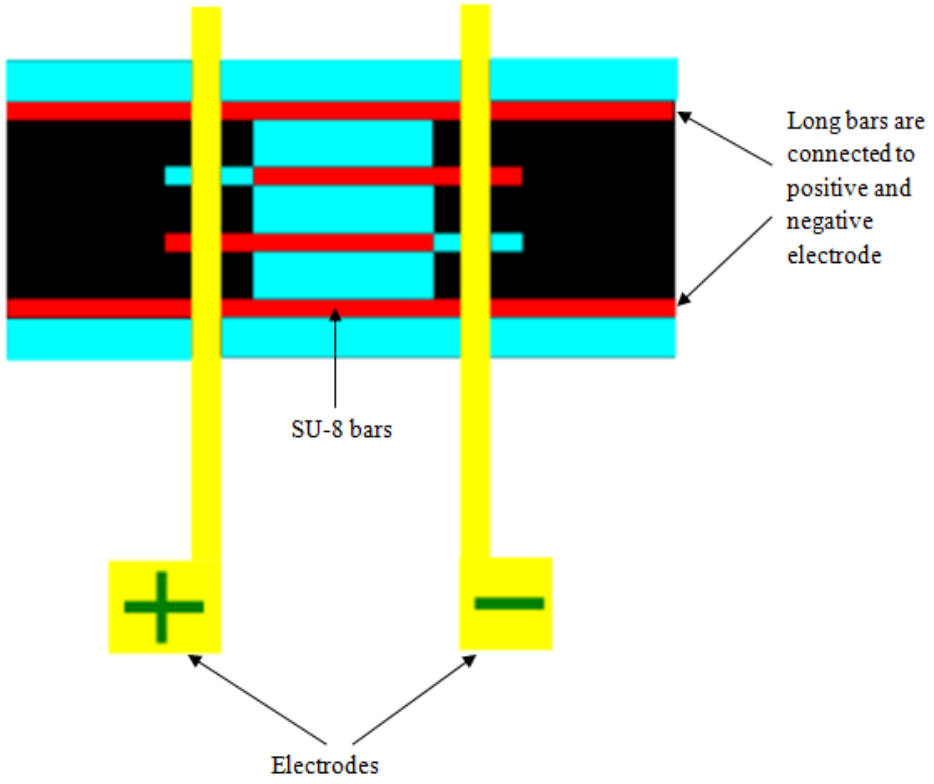

Figure 34. The long polymer walls at the two ends of the channel are connected to the positive and negative electrode hence, shorting the entire structure.

As seen in Figure 35 (a), the long SU-8 fins at the two ends of the channel are not connected. Hence, there is no internal shorting between the electrodes. The coated area of the substrate with metal and the fins are connected to the L-shaped electrodes that have extended

outside the channel. The '+' and '– sign indicate the positive and negative electrode respectively. The electrodes are positioned at the opposite ends of the channel so that there is no shorting externally. Figure 35 (b) shows the dimensions of the new channel.

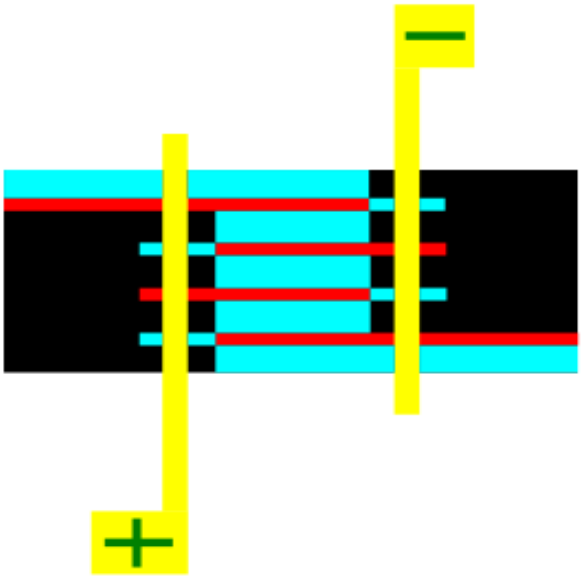

(a)

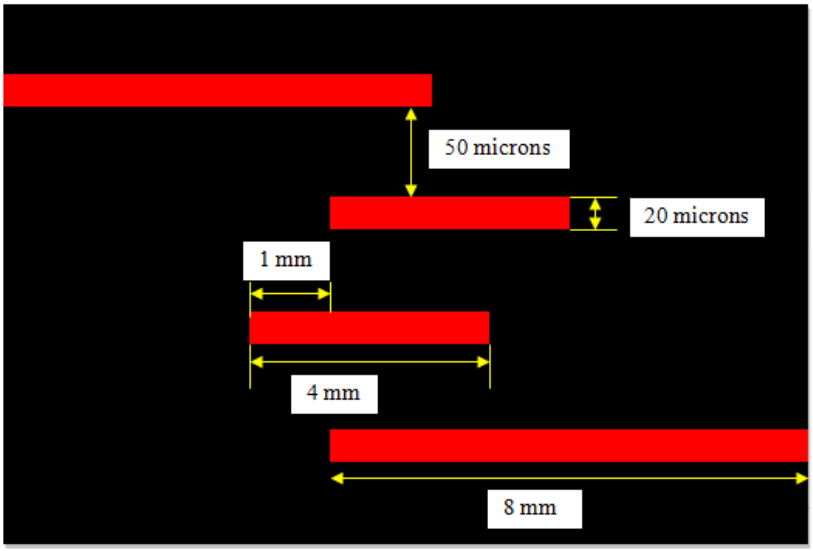

(b)

Figure 35. Change in channel pattern and dimensions. (a) Microfluidic channel with reduced length of polymer walls at the two ends of the channel. (b) Dimensions of the polymer bars (Figure not to scale).

In the new channel thus formed, the spacing between the consecutive bars is 50 microns with the width of each wall being 20 microns. The consecutive bars are shifted from each other by 1 mm and the length of the bars is 4 mm. The two long bars at the end are 8 mm long.

4.6 Optical Microscope Images showing Metal Coating

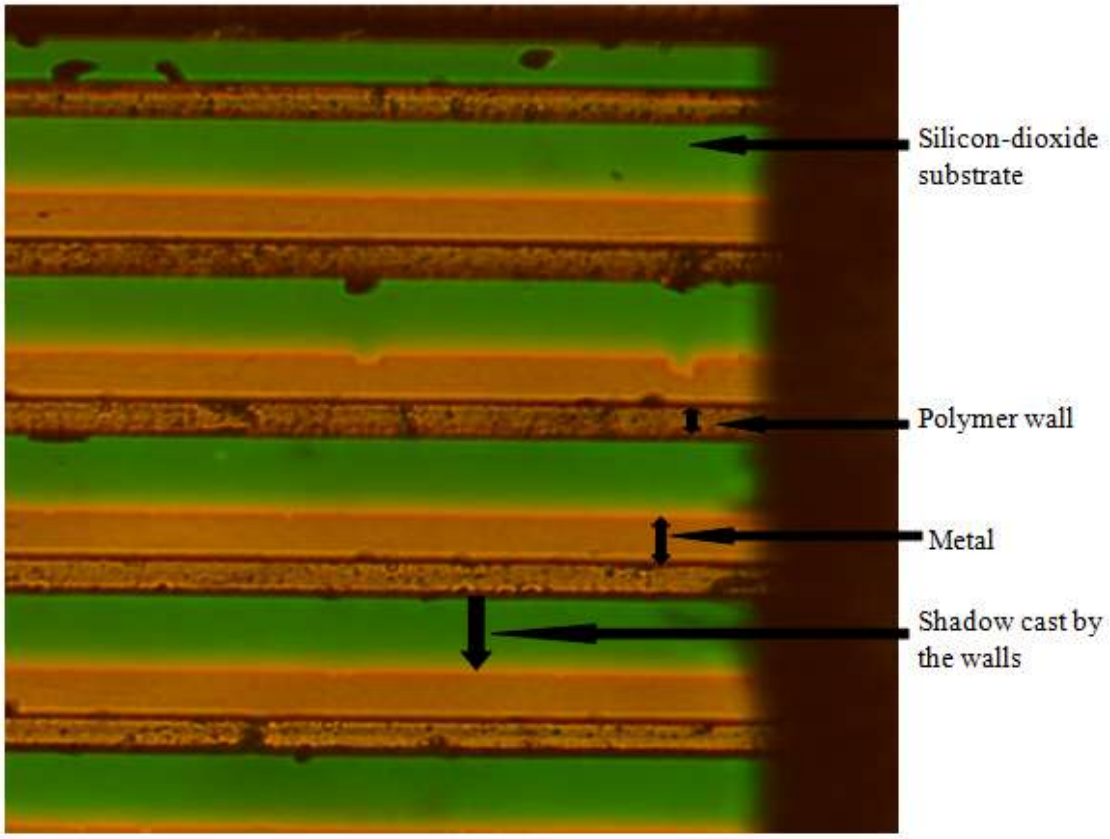

Figure 36. Single-sided angular evaporation. The substrate is tilted at an angle on one side to cast shadow.

Figure 36 shows shadow casted by the SU-8 fins due to single-sided angular evaporation. The resist is around 52 microns tall as measured by the profilometer and the spacing between the SU-8 fins is 120 microns. The angle set in the equipment was 55^0 so that the 52 microns tall structure will cast a shadow up to 75 microns. Hence, we see that the SU-8 walls have casted a

shadow thus preventing any region up to 75 microns from receiving metal. This is observed by the line separating the two regions. The dirt particle on the fins have also casted a shadow, indicating the accuracy of the shadowing effect.

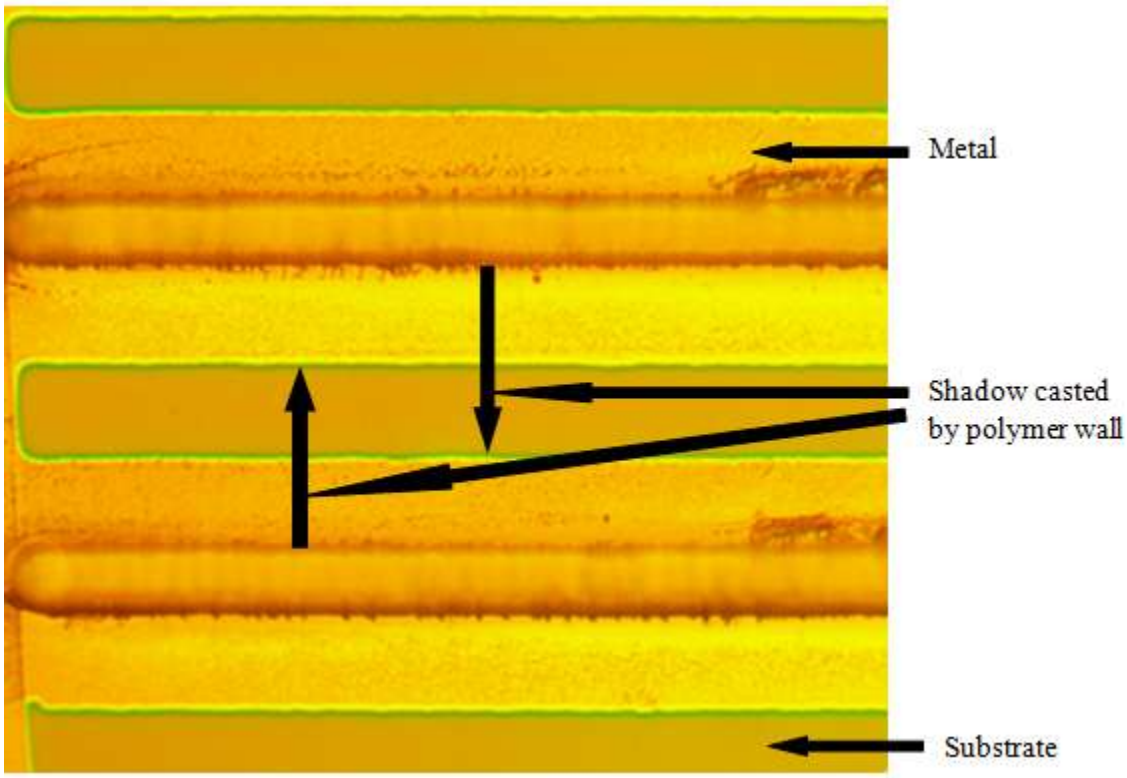

Figure 37. Double sided angular evaporation. The substrate is tilted at an angle on both the sides to cast shadows.

Figure 37, shows double-sided angle evaporation as compared to the single-sided evaporation in Figure 36. Each fin is surrounded by a film of metal and there is a gap between the two metal films which comprises of silicon dioxide substrate. The substrate was tilted on one side to 55^0 so that the 52 microns tall structure would thus cast a shadow up to 75 microns. The substrate was then tilted to 55^0 on other side so that the fin will cast a shadow on its opposite side. Two shadows are hence cast by the SU-8 pillars due to tilting the substrate by the same angle on both the sides.

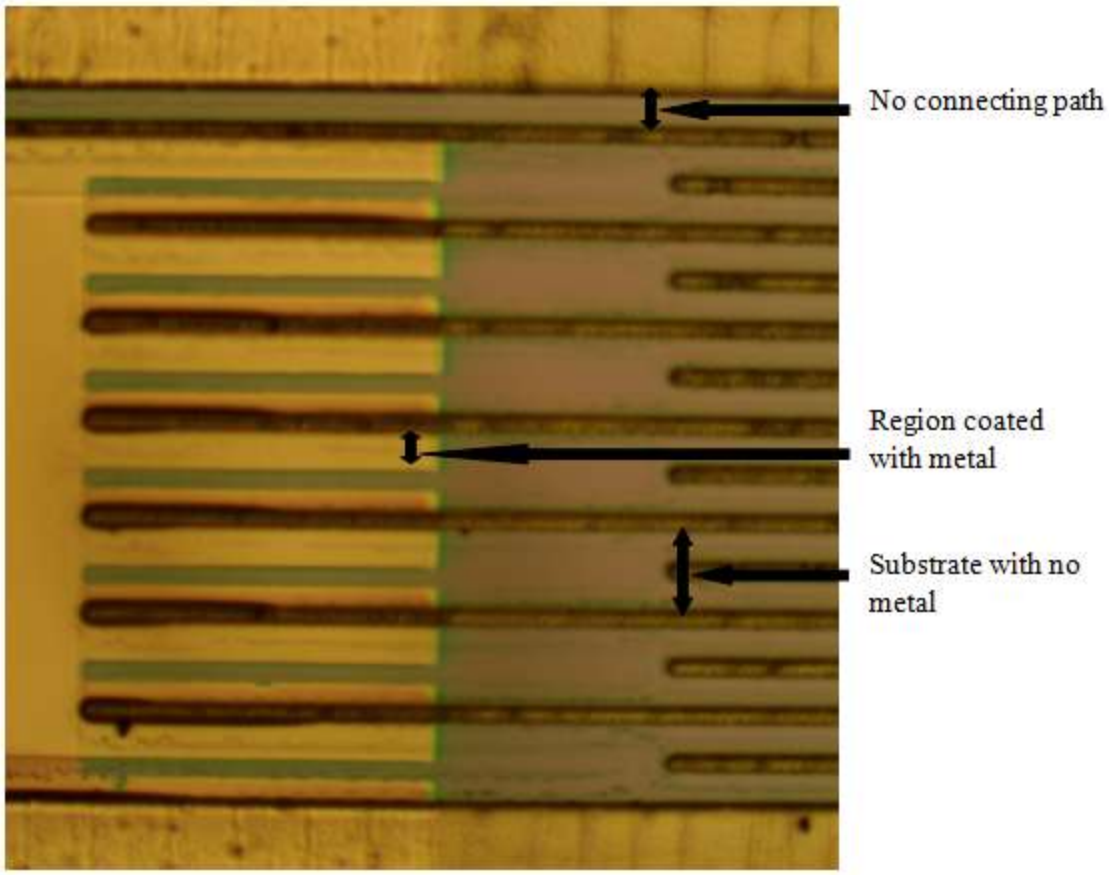

Figure 38. Alternate fins are connected to metal. There is no metal connecting the long polymer bar at the end and the boundary of the channel.

Figure 38 shows fins that have casted shadows to form a continuous connection of metal. There is no metal between the long bar at the end and the metal coated substrate thus, assuring that there is no electrical contact between them. This was possible only because of the shadowing effect of the SU-8 fins. The shadow casts by the fins are not equal on both sides since the tilting of the substrate on one side was larger than the other hence casting a longer shadow. However, it does not matter as long as the shadow cast is greater than 70 microns which is the sum of spacing between fins and width of fins. Hence, the angle on one side has casted a shadow up to 60 microns whereas the angle on the other has casted a shadow up to 90 microns.

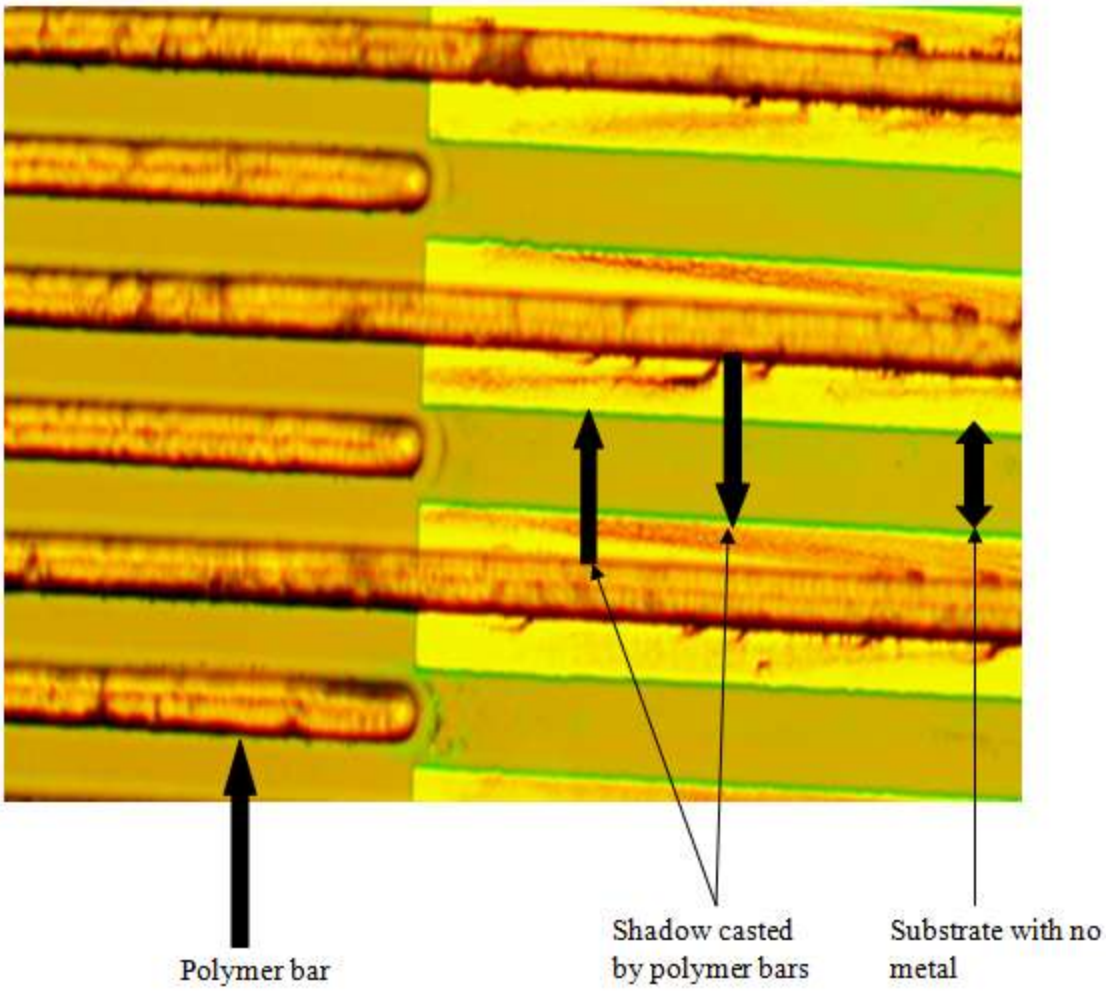

Figure 39. Coated channel walls formed by double-angle evaporation.

Figure 39 shows the shadows cast by the channel walls. The shadows cast also appear to be very sharp. The channel walls are coated up to a depth which is decided by the angle of tilting the substrate in the electron beam evaporator equipment. In this case, the depth is 35 microns since the angle set in the equipment was 55^0. From the figure, we see that the alternate fins are covered by the metal and there is a gap of non-coated metal region between the metal layers, which is the substrate. This indicates the shadows have been cast correctly and there is no metal between the adjacent fins.

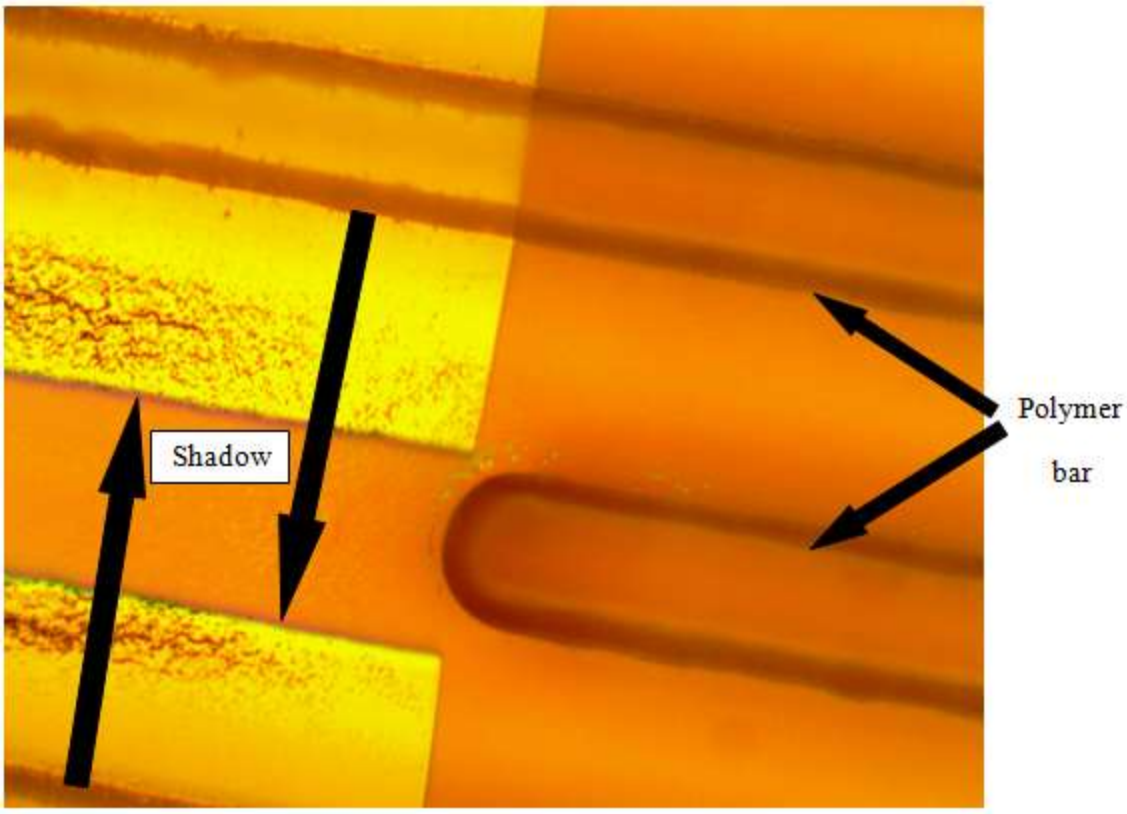

Figure 40. Zoomed image to ensure that adjacent walls are not connected.

The zoomed image of the electrodes in Figure 40 clearly shows that there is no contact between the adjacent fins. The two shadows are separated by a finite distance, which is the substrate region. This is also verified by calculating the length of the shadows that were casted by the SU-8 pillar. As the fins are spaced 50 microns apart and the width of the fins is 20 microns, the safe limit to cast shadows to assure no contact between adjacent fins is 70 microns. The casted shadow is greater than 70 microns which is clearly seen in the image. Since, the resist is 52 microns tall as measured by the profilometer and the casted shadow is approximately 75 microns which is calculated as the angle set in the equipment is known, the fins are coated to 65% of its height. The remaining 35% of the fin's height does not receive any metal.

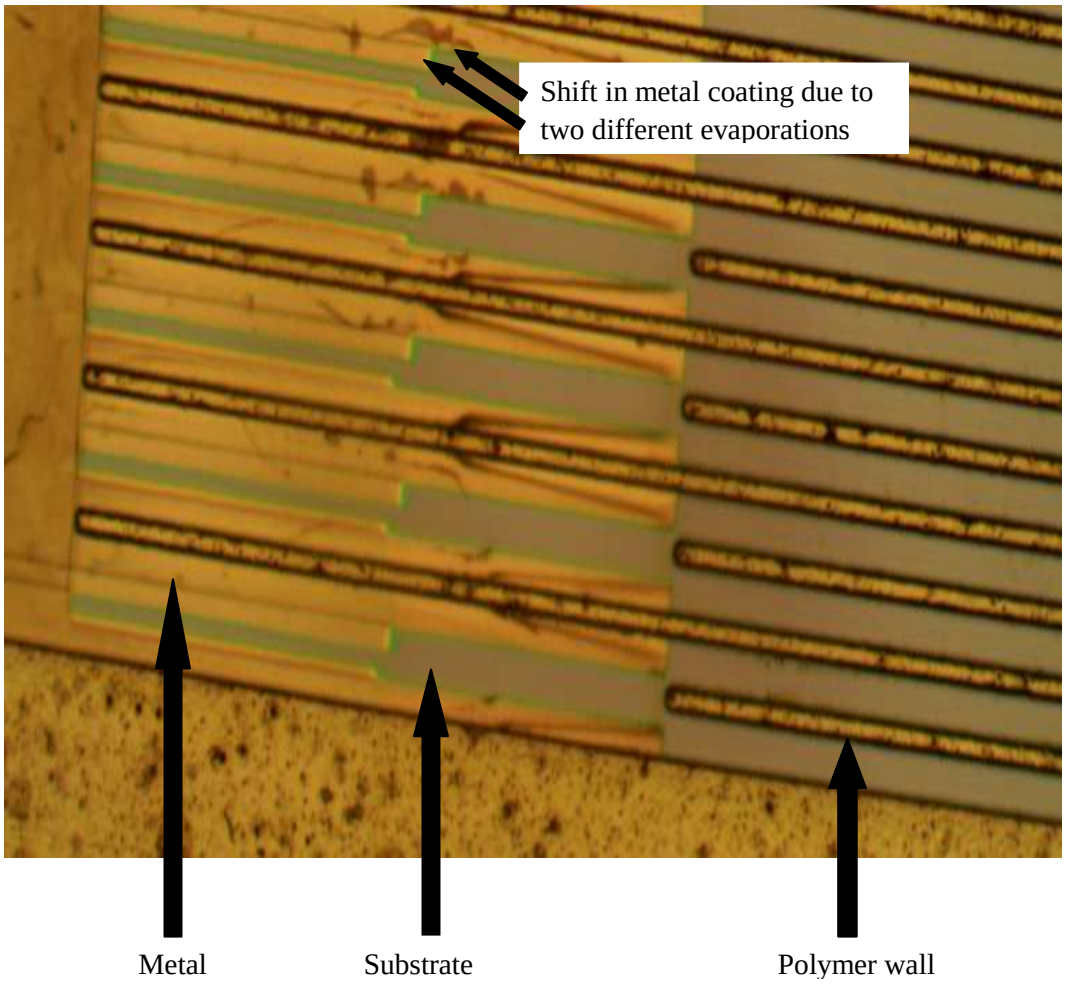

Figure 41. Image of electrodes obtained after performing two coatings of metal.

The integrated structure obtained after the two evaporation steps i.e., coating channel walls with metal and forming 'L' shaped electrodes is shown in Figure 41. Since, a lower angle was used to connect the alternate fins, it is seen that the shadows cast by the fins are up to 60 microns. A larger angle was used to coat channel walls and hence the shadows casted by the fins are up to 80 microns. Hence, there is a shift observed in the metal that is coated on the substrate which is the result of two evaporations at different angles. However, there is no shorting of the metal electrodes since there is no connecting path between adjacent shadows.

From the optical microscope images, it is seen that there is no shorting between adjacent walls. The metal has coated the polymer on the top and up to a certain depth but not the base or the spacing between the adjacent fins.

4.7 Resistance Measurement

After fabricating the microfluidic channel and coating metal on the channel walls to form electrodes, resistance of the liquid in the channel is measured. This is required to assure that the channel formed is not shorting internally. This is verified by first measuring air resistance i.e., having no liquid dispersed in the channel. The resistance of DI (de-ionized) water and conducting solution is measured later. The standard resistivity of DI water is 1 mega ohm-cm [33] and Phosphate Buffered Saline (PBS) solution has a standard conductivity of 0.015 mho/cm [34]. Due to high and low resistivity values of DI water and buffer solution, the resistance for the two solutions is expected to be high and low respectively. The resistance of liquid in the channel is measured by ohm-meter and its value is compared with the calculated resistance. The calculated value of resistance is obtained by

$$R = \rho L/A, \tag{4}$$

where, R = calculated value of resistance, ρ is the resistivity of liquid under measurement, L is spacing between the electrodes, and A is the effective area of contact for the liquid.

Initially, on measuring the resistance of air, no value was displayed on the ohm-meter as the maximum value that could be measured by the equipment was 20 MΩ. The calculated and observed resistance value for DI water was 30 MΩ and 6 MΩ respectively whereas for buffer solution it was 3 KΩ and 90 KΩ respectively. As seen from the calculated and observed values for the two liquids, DI water's resistance value is very high which is in the range of mega-ohms whereas the resistance value for buffer solution is very low and is in the range of kilo-ohms. Since, the resistivity value of DI water and buffer were high and low respectively, the calculated

resistance value for the two solutions is obtained accordingly. This is due to the resistance being directly proportional to the resistivity. The resistivity of air is very high in the order of 10^{16} ohm-m and hence its resistance could not be measured by the available ohm-meter equipment. The circuit behaves correctly as per expected which is confirmed from the observed and calculated values of air, DI water and buffer solution. Hence, the fabricated channel is not shorting, the electrodes formed are continuous and there is no break in the circuit.

Chapter 5

Summary and Future Work

The microfluidic channel has thus been fabricated via spin coating, pre-exposure bake, contact lithography, post-exposure bake, development of the resist, and double-sided angular metal evaporation. The fabrication process and parameters were modified to overcome several difficulties that were encountered during forming the channel. Under exposure issue was resolved by increasing exposure time, stress within the resist was resolved by changing dimensions of the channel and using a soft or pre-exposure bake step at two different temperatures, and shorting of the channel was resolved by decreasing length of the long polymer bars at the end. The channel obtained after eliminating the issues was devoid of any stress effects. After forming the channel, its walls were coated with metal to form contact electrodes.

The electrodes were formed with a technique known as double-angled evaporation which coated metal only on the channel walls to a certain depth. The depth of metal coating was decided by the angle set in the equipment. Two masks were required to perform the metal coating. First mask connected the alternate fins at each side to form ‘L’ shaped electrodes. The other mask was used to coat the channel walls and hence connect them to the electrodes that were formed by the first evaporation mask. The spacing between the fins and base of the fins did not receive any metal due to the shadows that were cast by the SU-8 polymer walls. There was no shorting of the channel walls which was verified visually and electrically. The images taken from the microscope gave a visual verification that the fabricated channel was not shorting as the shadows casted by the walls prevented any metal from coating the base of the wall as well as the spacing between the walls. However, electrical testing was required to ensure completely that the channel formed can be used for further analysis. This was done by measuring resistance of two standard solutions

whose resistivity was known. The resistance for air, DI water and buffer solution were observed across the ohm-meter. The values for DI water and PBS solution were calculated by using their standard resistivity values and channel dimensions. Air gave a very high resistance which could not be measured, DI water gave a very high resistance in mega-ohms and conducting solution gave a low resistance which was in kilo-ohms. Since the channel behaved as per expected it was thus, finally assured that the channel formed was non-shorting.

The future work in this project lies firstly in sealing the channel. One method of sealing the channel is by oxygen plasma bonding [35]. Once the channel is sealed, it can be assured that there will be no contamination from exposure to atmosphere while performing the experiment. Efficient cleaning techniques need to be developed to clean the channel and hence eliminate any kind of residue which remains on the substrate after developing the resist. The channel length can be scaled down to increase the sensitivity of the device however, stress issues need to be resolved.

Stainless steel masks should be used for evaporation as they are robust as compared to aluminum shim stock or plastic mask. Liquid can be made to flow through the channel by pumping, electrophoresis, capillary action or gravitational force. The two evaporation masks used can be integrated into one mask as shown in Figure 42. The L shaped electrode mask and the mask to coat the channel walls has been combined into one mask. This idea was thought since both the evaporations had to be performed at an angle and hence by tilting the substrate on both sides the electrodes are formed and channel walls are coated in the same evaporation step. This reduces time for coating metal on channel walls. Chromium can be replaced with gold as the metal for forming electrodes [21] using the procedure mentioned in this project since, ECL has been demonstrated with gold electrodes in a microfluidic channel. Also to test ECL, a photomultiplier tube (PMT) is required since for lower reagent volumes the intensity of the signal may be low and hence it can be enhanced with the use of a PMT. An ECL solution will be required and the voltage needs to be incremented in steps to determine the threshold voltage for

ECL. Thus, the device formed can be tested to serve its purpose of being an electrochemiluminescence sensor.

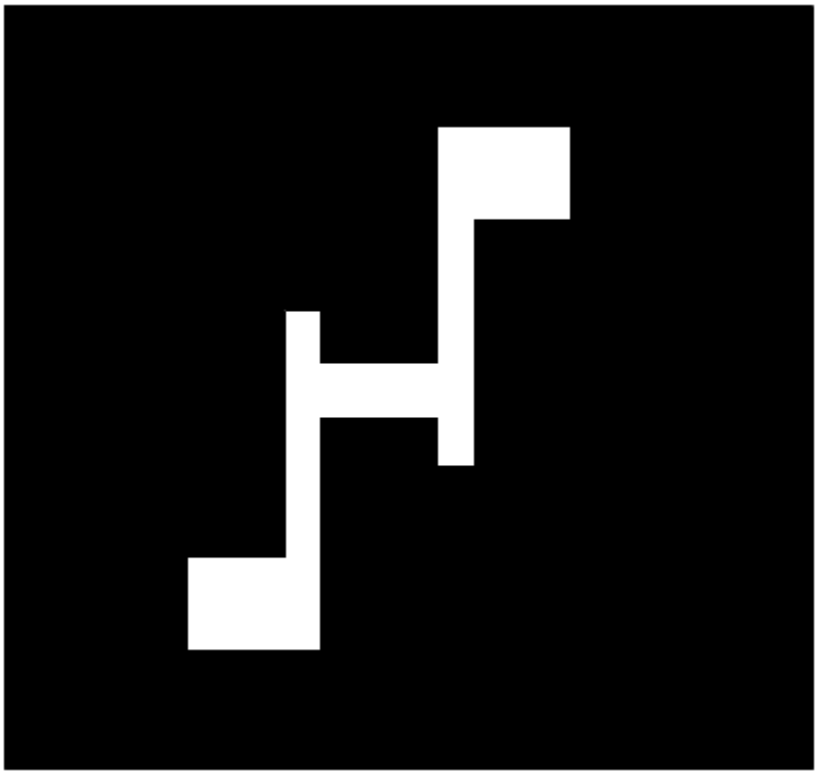

Figure 42. Single evaporation mask for forming electrodes and to coat channel walls.

A low-cost and fast technique of forming microchannels was demonstrated in this project. The sensitivity of the device is also very high due to several inter-digitated arrays of metal electrodes. The electrodes formed were 50 microns tall hence, providing larger area for liquid to interact with the channel walls. Thus, utilizing one photoresist, and a simple lithography and metal evaporation step, a prototype for an ECL sensor was fabricated.

References

[1] E. Verpoorte and N. Rooij. “Microfluidics Meets MEMS,” *Proceedings of the IEEE*, Vol. 91, No.6, June, 2003.

[2] Yager lab, Eric Schilling. Basic Microfluidic Concepts, Sept. 7, 2001. Retrieved Sept. 11, 2011, from faculty.washington.edu/yagerp/microfluidicstutorial/basicconcepts/basicconcepts.htm.

[3] D. Erickson, D. Li. “Integrated microfluidic devices,” *Analytica Chimica Acta 507*, pp. 11–26, 2004.

[4] G. Fiorini and D. Chiu. “Disposable microfluidic devices: fabrication, function, and application,” *BioTechniques*, Vol. 38, No. 3, pp. 429-446, March 2005.

[5] MEMS encyclopedia. SU-8: Thick Photo-Resist for MEMS. Retrieved June 6, 2011, from memscyclopedia.org/su8.html.

[6] H. Lorentz, M. Despont, N. Fahrni, N. LaBianca, P.Renaud, and P.Vettiger. “SU 8: a low-cost negative resist for MEMS,” *Journal of Micromechanics and Microengineering*, Vol. 7, pp. 121–124, 1997.

[7] A. Campo and C. Greiner. “SU-8: a photoresist for high-aspect-ratio and 3D submicron lithography,” *Journal of Micromechanics and Microengineering*, Vol. 17, pp. R81–R95, 2007.

[8] T. Vo-Dinh and B. Cullum. “Biosensors and biochips: advances in biological and medical diagnostics,” *Fresenius Journal of Analytical Chemistry*, Vol. 366, pp. 540–551, 2000.

[9] D. Gatto-Menking, H. Yu, J. Bruno, M. Goode, M. Miller, and A. Zulich. “Sensitive detection of biotoxids and bacterial spores using an immunomagnetic electrochemiluminescence sensor,” *Biosensors & Bioelectronics*, Vol. 10, pp. 501-507, 1995.

[10] G. Blackburn, H. Shah, J. Kenten, J. Leland, R. Kamin, J. Link, J. Peterman, M. Powell, A. Shah, D. TaHey, S. Tyagi, E. Wilkins, T. Wu, and R. Massey. “Electrochemiluminescence

Detection for Development of Immunoassasys and DNA Probe Assays for Clinical Diagnostics," *Clinical Chemistry*, Vol.37, No. 9, pp. 1534-1539, 1991.

[11] BC. Mathew, RS. Biju, and N. Thapalia. "An overview of electrochemiluminescent (ECL) technology in laboratory investigations," *Kathmandu University Medical Journal*, Vol. 3, No. 1, Issue 9, pp. 91-93, 2005.

[12] A. Lee, P. Burke, and J. Brody. "Electrochemiluminescence as a tool for microscopy at the nanoscale," *Proceedings of the SPIE*, Vol. 5331, pp. 13-20, 2004.

[13] M. Richter. "Electrochemiluminescence (ECL)," *Chemical Reviews*, Vol. 104, No.6, pp. 3003-3036, 2004.

[14] H. Chu, J. Yan, and Y. Tu. "Study on a Luminol-based Electrochemiluminescent Sensor for Label-Free DNA Sensing," *Sensors*, Vol. 10, pp. 9481-9492, 2010.

[15] L. Hu and G. Xu. "Applications and trends in electrochemiluminescence," Chemical Society Reviews, Vol. 39, pp. 3275-3304, 2010.

[16] Q. Li and X. Zhou. "Sensitive detection and quantitation of EZH2 expression in cancer cell by an electrochemiluminescent method," *Proceedings of SPIE*, Vol. 7519, pp. 75191J1-J7, 2009.

[17] R. Wilson, C. Clavering, and A. Hutchinson. "Paramagnetic bead based enzyme electrochemiluminescence immunoassay for TNT," *Journal of Electroanalytical Chemistry*, Vol. 557, pp.109-118, 2003.

[18] K.Baker, M. Rendall, A. Patel, P. Boyd, M. Hoare, R. Freedman, and D. James. "Rapid monitoring of recombinant protein products: a comparison of current technologies," *Trends in Biotechnology*, Vol.20, No.4, pp. 149-156, April 2002.

[19] L. Wang, L. Flanagan, and A. Lee. "Side-Wall Vertical Electrodes for Lateral Field Microfluidic Applications," *Journal of Microelectromechanical Systems*, Vol. 16, No. 2, pp. 454-461, April 2007.

[20] M. Wu, B. Xu, H. Shi, J. Xu, and H. Chen. "Electrochemiluminescence analysis of folate receptors on cell membrane with on-chip bipolar electrode," *Lab Chip*, Vol. 11, pp. 2720-2724, 2011.

[21] P. Pittet, G. Lu, J. Galvan, R. Ferrigno, L. Blum and B. Leca-Bouvier. "PCB-based integration of electrochemiluminescence detection for microfluidic systems," *Analyst*, Vol. 132, pp. 409–411, 2007.

[22] Microchem Corporation. SU-8 2000 Permanent Epoxy Negative Photoresist Processing Guidelines for SU-8 2050. Retrieved Feb. 17, 2011 from www.microchem.com/pdf/SU-8 2000DataSheet2025thru2075Ver4.pdf.

[23] Brewer Science. Spin Coater Theory. Retrieved Feb. 2, 2011, from www.brewerscience.com/research/processing-theory/spin-coater-theory.

[24] G. Shao. "Polymer Based Microfabrication and its applications in Optical Mems and Biomems," Ph.D. dissertation, Dept. Engineering Science, Louisiana State Univ., 2011.

[25] Photolithography. Retrieved August 25, 2012 from www.ece.gatech.edu/research/labs/vc/theory/photolith.html.

[26] A. Hawkins. Contact Photolithographic Alignment Tutorial, Jan., 2004. Retrieved July 20, 2012 from www.cleanroom.byu.edu/alignment.parts/Alignment_Tutorial.pdf.

[27] IBM. Lithography materials, Chemically Amplified Resists. Retrieved Sep. 1, 2012 from researcher.watson.ibm.com/researcher/view_project_subpage.php?id=3662.

[28] Omega Optical. Filters for Photolithography. Retrived May 25, 2011 from www.horiba.com/fileadmin/uploads/Scientific/glenspectra/Documents/Filters/Filters_for_ Photolithography_Flyer.pdf.

[29] Midwest Tungsten Service. Electron Beam Evaporation. Retrieved August 5, 2012 from www.tungsten.com/tipsbeam.pdf.

[30] P. Yuen and V. Goral. "Low-cost rapid prototyping of flexible microfluidic devices using a desktop digital craft cutter," *Lab Chip*, Vol. 10, pp. 384-387, 2010.

[31] D. Hwang, Y. Lo, and K. Chin. “Development of a systematic recipe set for processing SU8-5 photoresist,” 2001.

[32] Microchem Corporation. SU-8 2000 Permanent Epoxy Negative Photoresist Processing Guidelines for SU-8 2005. Retrieved June 1, 2011 from microchem.com/pdf/ SU-82000DataSheet2000_5thru2015Ver4.pdf.

[33] Radiometer Analytical SAS. Conductivity Theory and Practice. Retrieved August 23, 2012 from www.analytical-chemistry.uoc.gr/files/items/6/618/agwgimometria_2.pdf.

[34] Fisher Bioreagents. Phosphate buffered Saline solution. Retrieved August 17, 2012 from extranet.fisher.co.uk/webfiles/uk/web-docs/450_CH.pdf.

[35] S. Serraa, A. Schneidera, K. Maleckib, S. E. Huqa, and W. Brennerb. “A simple bonding process of SU-8 to glass to seal a microfluidic device,” presented at the *4M 2007* Conf., Borovets, Bulgaria, 2007.